DISSERTATIONS IN
FORESTRY AND
NATURAL SCIENCES

Tapani Hirvonen

A Wide Spectral Range Imaging System

- Applications in Wood Industry

Publications of the University of Eastern Finland
Dissertations in Forestry and Natural Sciences

UNIVERSITY OF
EASTERN FINLAND

TAPANI HIRVONEN

A Wide Spectral Range Imaging System

Applications in Wood Industry

Publications of the University of Eastern Finland
Dissertations in Forestry and Natural Sciences
No 173

Academic Dissertation
To be presented by permission of the Faculty of Science and Forestry for public examination in the Auditorium AU100 in Aurora Building at the University of Eastern Finland, Joensuu, on March, 13, 2015,
at 12 o'clock noon.

Department of Physics and Mathematics

Kopio Niini Oy
Helsinki, 2015
Editors: Prof. Pertti Pasanen, Prof. Kai–Erik Peiponen,
Prof. Matti Vornanen and Prof. Pekka Kilpeläinen

Distribution:
University of Eastern Finland Library / Sales of publications
P.O.Box 107, FI–80101 Joensuu, Finland
tel. +358–50–3058396
julkaisumyynti@uef.fi
http://www.uef.fi/kirjasto

ISBN: 978-952-61-1724-9 (printed)
ISSNL: 1798-5668
ISSN: 1798-5668
ISBN: 978-952-61-1725-6 (pdf)
ISSNL: 1798-5668
ISSN: 1798-5676

Author's address:
University of Eastern Finland
Department of Physics and Mathematics
P.O.Box 111
80101 Joensuu, FINLAND
email: tapani.r.hirvonen@uef.fi

Supervisors:
Professor Markku Hauta–Kasari, Ph.D.
University of Eastern Finland
School of Computing
P.O.Box 111
80101 Joensuu, FINLAND
email: markku.hauta–kasari@uef.fi

Professor Kai–Erik Peiponen, Ph.D.
University of Eastern Finland
Department of Physics and Mathematics
P.O.Box 111
80101 Joensuu, FINLAND
email: kai.peiponen@uef.fi

Mika Sorjonen, Ph.D.
Palomäentie 4
88620 Korholanmäki, FINLAND
email: sorjonen.mika@gmail.com

Reviewers:
Professor Frank Lam, Ph.D.
The University of British Columbia
Department of Wood Science
Forest Sciences Centre 4041, 2424 Main Mall
BC V6T 1Z4, Vancouver, CANADA
email: frank.lam@ubc.ca

Associate professor Barry Cense, Ph.D.
Utsunomiya University
Center for Optical Research and Education
7–1–2 Yoto
321-8585 Utsunomiya, JAPAN
email: bcense@cc.utsunomiya–u.ac.jp

Opponents:
Professor Erkki Verkasalo, Dr.Sc. (Agr.&For.)
Natural Resources Institute Finland (Luke)
P.O.Box 68
80101 Joensuu, FINLAND
email: erkki.verkasalo@luke.fi

Adjunct professor Juha Toivonen, D.Sc. (Tech.)
Tampere University of Technology
Department of Physics
P.O.Box 692
33101 Tampere, FINLAND
email: juha.toivonen@tut.fi

ABSTRACT

In this study a wide spectral range (200–2500 nm) imaging system with photoluminescence imaging capability is introduced. The setup is developed from three different line spectral cameras by merging them to operate simultaneously in order to achieve savings in measuring time and sample handling. The system is benchmarked to obtain knowledge about an appropriate operational range and performance. Findings indicate that the developed system has the most significant challenges in the ultraviolet region.

The system is then used to obtain a public spectral image database from Nordic sawn timber for research purposes. The selected wood species are birch (*Betula* sp.), Norway spruce (*Picea abies*) and Scots pine (*Pinus sylvestris*). In all, 107 samples including several different surface features (e.g. knots and decay) are measured in frozen, melted and room–dried conditions to correspond to real production circumstances in sawmills across seasons. This results in the final database containing approximately 44 million spectra in which the potential is demonstrated with an analysis example of fluorescent area extraction, retrieval of the spatial distribution of aromatic lignin and simplified MC detection. According to the results, the spectral image database offers a possibility to observe spatial distributions of different wood properties.

Finally, the imaging system is applied to develop a practical, non–contact and non–destructive method for the layer thickness measurement of freshly applied water–dilutable compounds, for example, adhesives used in the production of glued wood. The absorption peaks of water are associated with the layer thickness of the compounds under examination. From these key wavelengths a method is derived which requires the observation of only two wavelengths.

Universal Decimal Classification: 535.33, 535.37, 543.42, 681.785, 620.179.1, 691.11
Library of Congress Subject Headings: Optical measurements; Spectral imaging; Spectrum analysis; Spectral reflectance; Fluorescence; Photolu-

minescence; Nondestructive testing; Thickness measurement; Wood; Laminated wood; Timber; Quality control; Engineering inspection
Yleinen suomalainen asiasanasto: spektrikuvaus; spektrianalyysi; fluoresenssi; fotoluminesenssi; rikkomaton aineenkoetus; puuteollisuus; sahatavara; liimapuu; laadunarviointi; laadunvalvonta

Preface

First, my deepest gratitude is given to my supervisor, Prof. Markku Hauta–Kasari, for supervising this thesis and past research projects. I wish to also thank him from granting me this opportunity to work in this field and research group over the years. I have had the pleasure to note the possibilities this versatile basis of spectral color research can offer. I am also deeply grateful to Mika Sorjonen for supervising me in matters concerning the wood industry, and Prof. Kai–Erik Peiponen for supervising me in spectroscopy. I would like to thank the reviewers of my thesis, Prof. Frank Lam and Associate prof. Barry Cense, for their professional and constructive feedback.

My humblest gratitude to the North Karelia Regional Fund of the Finnish Cultural Foundation and Puumiesten Ammattikasvatussäätiö for supporting this work financially. I am grateful to the TimTekno research program for this interesting topic and its members for fruitful collaboration. I would like to thank all my co–authors for their valuable feedback and contribution. I wish to also thank Prof. Jaume Pujol and his color group at the Polytechnic University of Catalonia for the opportunity to work with them during my exchange period.

I would like to acknowledge my past and present colleagues in the Institute of Photonics, in the SIB Labs and in the Spectral Color Research Group who have aided me in achieving my major goal and with whom I have had a pleasure to work. Special thanks to Jussi Kinnunen, Jukka Antikainen, Niko Penttinen, Jouni Hiltunen and Ville Heikkinen.

I am thankful to my parents, Saara and Mauri for their endless

support. Furthermore, I want to express my thanks to my sisters and friends for the great time that we have had together. Finally, special thanks to my beloved Piia for her encouragement and love.

Joensuu, February 27, 2015

Tapani Hirvonen

"There was a sculptor. He found this stone, a special stone. He dragged it home and he worked on it for months until he finally finished it. When he was ready he showed it to his friends. They said he had created a great masterpiece, but the sculptor said he hadn't created anything. The statue was always there, he just chipped away the rough edges."

– Colonel Sam Trautman,
Rambo III (1988)

LIST OF PUBLICATIONS

This thesis consists of the following selection of the author's publications:

I T. Hirvonen, N. Penttinen, M. Hauta–Kasari, M. Sorjonen and K.–E. Peiponen, "A Wide Spectral Range Reflectance and Luminescence Imaging System," *Sensors* **13,** 14500–14510 (2013).

II T. Hirvonen, J. Orava, N. Penttinen, K. Luostarinen, M. Hauta–Kasari, M. Sorjonen and K.–E. Peiponen, "Spectral image database for observing the quality of Nordic sawn timbers," *Wood Sci. Technol.* **48,** 995–1003 (2014).

III T. Hirvonen, N. Penttinen, M. Hauta–Kasari, M. Sorjonen and K.–E. Peiponen, "Near–infrared imaging method for measuring the thickness of water–dilutable turbid layers," *J. Imaging Sci. Technol.* **58,** 105031–105034 (2014).

Throughout the overview, these papers will be referred to by Roman numeral. The papers have been included at the end of this thesis with the permission of the copyright holders. In addition, the author has also participated in the preparation of other peer–reviewed papers [1,2].

SUMMARY OF PUBLICATIONS AND CONTRIBUTIONS

The publications selected in this dissertation are original research papers on spectral imaging and its applications.

Paper **I** deals with development of a wide spectral range imaging system. The need for the development process arose from the practical needs of Paper **II**, because a comprehensive database could only be measured with a sophisticated system. Later the system was also used for the measurements in Paper **III**. The idea of sensor fusion came from within a project group. System design, implementation and testing were performed by the author. Programming for the system control was done by Niko Penttinen. The author wrote the manuscript and the co–authors improved it with their feedback.

Paper **II** introduces a public spectral image database of Nordic sawn timbers for research purposes. It includes sample management, data acquisition and processing. Following the database specifications, the paper demonstrates the potential of the database with examples from couple analysis. The idea for the database came from a research project in which the author also contributed to database design. Samples were cut and prepared by Jorma Heikkinen. Measurements and data collection were performed by the author. Joni Orava, Ph.D., executed post processing for the acquired data and Katri Luostarinen, Ph.D., confirmed the surface features of the samples. The manuscript was written by the author.

Paper **III** presents the development process of a method for measuring the layer thickness of water–dilutable compounds. Key wavelengths associated with layer thickness were found using spectral imaging and analysis. As a result, an empirical model which uses the resulting wavelengths is derived and tested for the task. The research problem arose from the practical needs of a company inside the project group. The measurement design and execution were performed by the author. The idea for the use of the wavelength ratio came from Prof. Kai–Erik Peiponen, and created the foundation for the empirical model developed by the author. The

author wrote the manuscript and the co–authors contributed to the improvement process.

LIST OF ABBREVIATIONS

a.u.	Arbitrary unit
EM	Electromagnetic
GUI	Graphical user interface
IR	Infrared range of electromagnetic spectrum
LP	Line pair
MC	Moisture content compared to dry weight
PV	Polyvinyl
RGB	Red–green–blue
RH	Relative humidity
PSF	Point spread function
PSNR	Peak signal to noise ratio
SPD	Spectral power distribution
STD	Standard deviation
UV	Ultraviolet range of electromagnetic spectrum
VIS	Visible range of electromagnetic spectrum

NOTATION

A_{log}	Absorbance
A	Absorptance
α	Attenuation coefficient
C	Spectral response of sensor
c	Speed of electromagnetic radiation in vacuum
d	Thickness of object
E	Energy
h	Planck's constant
I_0	Incident ray
I_R, I_T, I_A	Reflected, transmitted and absorbed intensity
k	Concentration
L	Photoluminescence
R	Reflectance
r	Ratio of two wavelengths
S_D	Signal offset
S_R	Reference signal
S_S	Sample signal
T	Transmittance
λ	Wavelength
(x, y, z)	Spatial coordinates

Contents

1 Introduction

Nowadays wood is measured and evaluated many times during a production chain from recently planted forest to end product. These measurements provide information about the properties of wood, for example, quality and quantity, which are essential for profitability. At the same time technological progress generates new possibilities to develop novel measuring methods and techniques. In the future, these measuring methods will make it possible to produce products of higher quality, which are crucial in an open and free market.

Optical methods have been found to have substantial potential as a measuring technology since they are rapid and can perform measurements without contact. Optical methods are usually non–destructive in preserving samples and require minimal sample preparations. In the wood industry context gray scale cameras have initially been used in the imaging quality control of sawn timber. Then three–channel color cameras were employed. The next step could be the use of spectral cameras providing extremely accurate spectral information.

In recent decades several researchers and research groups around the world have studied wood using optical methods in order to determine non–destructive means to detect the properties of wood; they are faster and cheaper than traditional methods such as wet chemistry [3, 4]. Using present knowledge, for example, reaction wood, sapwood, early wood, late wood, knots, resin and wane can be detected with the visible (VIS) range of the electromagnetic (EM) spectrum [5–8].

The infrared (IR) region of the EM spectrum also holds considerable potential for wood research. This has previously been reported to be valid for wood species separation, decay process monitoring, blue stain and decay detection [9–13]. In addition, density, microfibril angle, fiber length and such mechanical properties of

wood as dynamic modulus of elasticity and bending strength have been examined [14–16]. Furthermore, chemical properties, for example, lignin and cellulose content and pulp yield can be resolved using infrared radiation [15, 17–20].

The ultraviolet (UV) region of the EM spectrum is also used in wood research, chiefly with photoluminescence. UV methods have been reported to be suitable for heartwood/sapwood ratio extraction, compression wood detection and wood species classification [1, 21, 22]. However, despite these numerous and versatile methods, challenges still exist, for example, with the moisture content detection of wood and gluing process management, which will be introduced in the next paragraphs.

Compared to the dry weight of fresh lumber moisture content (MC) varies between 20–180 % and this large variation makes the drying process challenging. At present, all boards are stacked and dried together regardless of their different initial MC. Thus, boards with a small initial MC will be dried unnecessarily long and boards with high initial MC may not be dried sufficiently. This could be avoided if the MC of freshly cut boards were somehow measured. The boards could then be classified by moisture classes according to their MC before the drying process. Hence, boards could be dried sufficiently which optimizes the drying process. This would mean savings in time, cost and energy and yield products with a more homogeneous quality. In some cases, board classification according to MC content could require modifications in the saw line. In most previous MC studies, the full near–infrared spectrum has been used with partial least squares regression to predict MC [4, 23, 24]. This method is relatively rigorous and requires expensive spectral sensors which limit practical applications and implementations.

In glued wood production the amount of adhesive and uniform layer thickness affect the quality of the end products and production costs. Nowadays adhesive can be applied using several methods such as curtain or extruder coating [25]. However, none of the applied methods can guarantee full adhesion in every single location of the glued surface. The lack of or insufficient amount

of adhesive decreases the strength properties of the end product whereas an excessive amount causes material losses and aesthetic harm when the adhesive gushes from joints. Of course, gushed adhesive can be planed or sanded away, which would take extra time and would be costly. Currently, the amount of adhesive on the surface is verified by weighing the object with and without adhesive [26]. Weighing is a slow process and ignores the spatial distribution of the adhesive on the surface. All these challenges could be overcome with an appropriate device capable of resolving information concerning adhesive layer thickness. This information makes it possible to monitor and control the application process of glued wood products, for example, to fix or reject a poorly glued part before compression, thus increasing the number of high quality products and optimizing production costs.

Water–dilutable polyvinyl (PV) based adhesives, commonly used in glued wood production, are visually white and highly light scattering. This makes it challenging to distinguish the thin layers of adhesive from the wood and therefore a precise machine vision measurement is difficult using traditional color cameras. Nonetheless, several methods for measuring film thickness have this far been developed and they are mainly based on reflectance or fluorescence. Reflectance methods compare the ratio of specular reflectance from an adhesive stripe and diffuse reflectance from the background material [27–29]. This method can be used to verify the existence of adhesives and the amount of adhesive can be approximated from the width of the stripe. A fluorescent method for detecting film thickness is based on the fact that emitted light is proportional to layer thickness within some thickness range [30]. Unfortunately, PV–based adhesives are not fluorescent enough for rapid and accurate measurement. This could be resolved by adding a fluorescent additive to the adhesive but it would increase costs and could decrease the strength properties of the adhesive.

Many machine vision groups around the world are capable of computationally detecting wood features. They do not, however, necessarily have the devices or resources to measure a compre-

hensive spectral image database for the process of developing new machine vision methods and techniques. With a spectral image database one could search key wavelengths which are associated with some specific feature (e.g. heartwood/sapwood), develop preprocessing and classification algorithms, develop transmission filters for cameras, optimize spectral power distributions of light sources and simulate detection processes [1,31]. Therefore, a publicly available and comprehensive spectral image database can be seen as a practical instrument for the development of wood material research. However, such a public database does not exist now.

All previously described cases could be approached with spectral imaging, which has shown its potential in different research fields [32–36]. Spectral imaging devices are able to simultaneously measure a spectrum from every target point. This saves a great deal of measuring time, which is a great advantage compared to devices which only measure from one point at a time. With this acquired spectral image information the spatial distributions of a feature under observation could be studied. From a practical point of view it would be convenient to have spectral data from as wide a wavelength range as possible, where all valid information is linked together pixel–wise. However, current spectral imaging devices have limitations in the ultra violet (UV) range of the EM spectrum and have not been used for photoluminescence imaging [33,36–40].

In this study, the structure presented in Fig. 1.1, a wide spectral range imaging system, is developed (Paper **I**), which is able to measure reflectance and photoluminescence. This system is then used to obtain a public spectral image database of Nordic sawn timber for research purposes (Paper **II**). The potential of the database is demonstrated with an example of fluorescent area extraction, retrieval of the spatial distribution of aromatic lignin and simplified MC detection. The wide spectral range imaging system is also used to develop a method for measuring the layer thickness of water–dilutable compounds (Paper **III**).

In the second chapter the aims of the study are stated. Chapter 3 expresses the optical framework and the concepts required

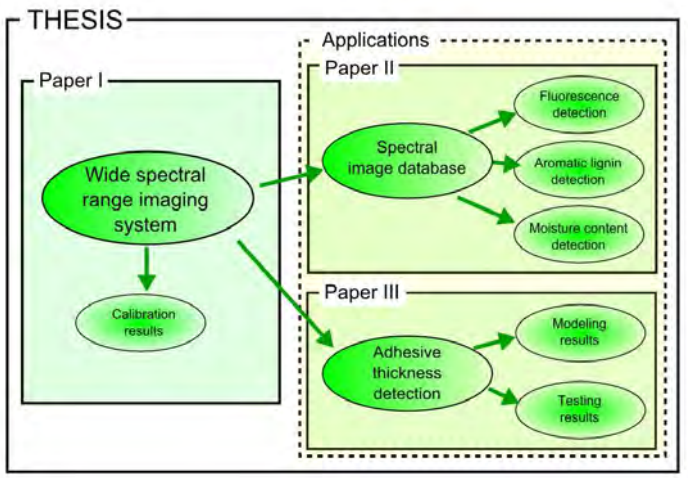

Figure 1.1: The structure of the thesis. Paper **I** *presents the wide spectral range imaging system developed in this work. Papers* **II** *and* **III** *concern the applications of developed system.*

in this work. Then, the key properties of adhesives and lumber are discussed and followed by an introduction of the materials and methods used. In chapter 5, the results are presented and considered against the aims of the study. Finally, the main findings are summarized in the conclusion.

2 Aims of the study

The aims of this study are the development of a wide spectral range imaging system and its practical applications in the context of the wood industry. The aims can be divided more precisely in to three parts as follows.

1. To develop and benchmark a wide spectral range imaging system for research purposes with a photoluminescence imaging ability from line spectral cameras available in the laboratory. At present, a device which is able to measure the 200–2500 nm wavelength range and photoluminescence is not available. This device is mainly developed for the work of the second aim.

2. To produce a public and comprehensive spectral image database of sawn timber for research purposes from the economically significant wood species of Finland [Scots pine (*Pinus Sylvestris*), Norway spruce (*Picea abies*), Birch (*Betula* sp.)]. At the moment, only three channel red–green–blue color image databases of wood material are available. Machine vision experts around the world may not have resources to measure high resolution spectral image data for the development process of new machine vision methods and techniques.

3. To develop a method for measuring the thickness of freshly applied adhesive in the production of glued wood. Currently, efficient method for thickness information extraction is not available even though it could increase the number of high quality products and optimize production costs.

3 Optical framework

Electromagnetic radiation can be divided in to several sub–types according to wavelength λ, as seen in Fig. 3.1. Human beings are able to see only the small 380–760 nm range of EM radiation called visible light and the best response is obtained around 550 nm [41,42]. Fortunately, technology makes it possible with spectroscopic methods to also observe other radiation types. EM radiation is usually presented with spectral power distribution (SPD), which describes power per unit area per unit wavelength. This SPD signal as a function of wavelength is generally called a spectrum. It should be noted in Fig. 3.1 that the energy of EM radiation is inversely proportional to wavelength. This knowledge is essential when later dealing with photoluminescence.

3.1 REFLECTANCE, TRANSMITTANCE AND ABSORPTANCE

Observation of the interaction between EM radiation and a material can reveal different properties from that material. A fundamental examination is executed, as seen in Fig. 3.2, by illuminating an object with a known ray I_0 and detecting the portions of the reflected I_R, transmitted I_T and absorbed I_A ray. According to the law of

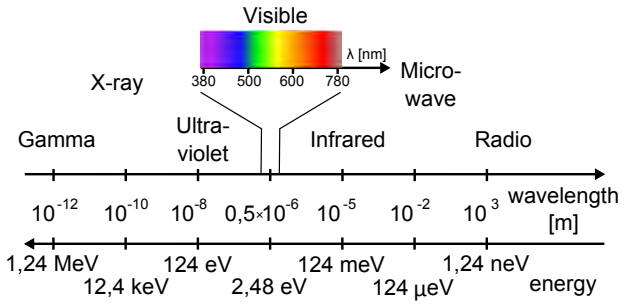

Figure 3.1: Electromagnetic spectrum where radiation is divided to sub–types according to wavelength and energy.

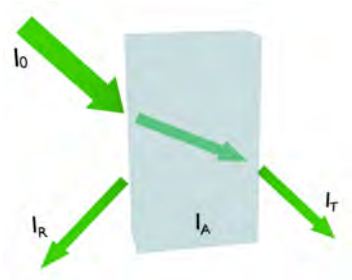

Figure 3.2: Interaction between EM radiation and a material. An incident ray I_0 is partly reflected, absorbed and transmitted.

conservation of energy $I_0 = I_R + I_T + I_A$ can be written when effects such as luminescence, Raman effect etc. are absent [43]. Furthermore, portions can be compared to the incident ray, i.e. I_R/I_0, I_T/I_0 and I_A/I_0, to retrieve factors for reflectance R, transmittance T and absorptance A respectively. Hence, for these factors 1 = R + T + A holds. For some applications it is also convenient to define absorbance A_{log} = -log(T), where the log is a 10–base logarithm. In practice, the reflectance factor is solved from

$$R = \frac{I_R}{I_0} = \frac{S_S - S_D}{S_R - S_D}, \tag{3.1}$$

where S_S is a measured signal from a sample, S_R a measured signal from a reference and S_D the offset of the sensor used. Naturally, this reflectance factor examination can be done for every spatial point (x, y) on the sample surface as a function of wavelength, thus R(x, y, λ).

3.2 LAMBERT–BEER LAW

Electromagnetic radiation which is transmitted inside some homogeneous substance, as seen in Fig. 3.2, attenuates an equal amount in every equally thick layer of the substance [44]. In other words, the magnitude of radiation will decrease exponentially as a function

of sample thickness d. Attenuation also depends on the concentration k of the substance. Thus, according to the Lambert–Beer law this relationship can be expressed as

$$A_{log} = \alpha kd, \tag{3.2}$$

where α is the material dependent attenuation coefficient. In this work concentration is assumed to be constant for the examined substances. It should be emphasized that the Lambert–Beer law is valid only where the linearity of Equation 3.2 holds. This can result in a limited thickness range for substances having high α values.

3.3 HYPERSPECTRAL IMAGING

Several techniques and commercial spectral imaging devices exist which are able to measure the previously mentioned R(x, y, λ) [45]. One such device is a line spectral camera (also known as a push broom spectral camera); its structure is presented in Fig. 3.3 [46]. There is a narrow slit immediately behind an objective which allows only rays from the one line of a sample plane to continue towards a sensor. Behind the slit, selected radiation progresses through a prism–grating–prism component which splits it in to a spectrum. Thus, every spatial point in the selected line has now its own spectrum, which is captured with the appropriate sensor. Since the sensor is able to see only one line at a time either the sample or the camera must be moved line by line to obtain the whole sample area.

Depending on the measuring geometry, sensor resolution and response it is possible to obtain extremely accurate spectral information from the sample with this line spectral device. Like the human eye, sensors are also able to operate only in some specific wavelength range. Similarly, operational sensitivity is not equal across the wavelength range and the spectral response C(λ) of the sensor is used to describe this inequality. The best response is usually achieved in the middle of operational range.

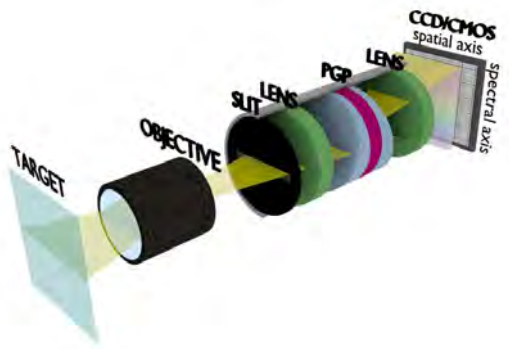

Figure 3.3: The principle of a line spectral camera. The target is imaged by the objective onto the slit, meaning that every point of the target is clearly in focus when it reaches the slit (image plane). The slit then selects only a single line of the target, which is then chromatically dispersed by the prism–grating–prism onto the sensor.

The measurement of R(x, y, λ) will produce a three–dimensional spectral image, which is demonstrated in Fig. 3.4. Each gray scale image in the stack presents the spatial distribution of the sample reflectance at some particular wavelength. From this spectral image it is possible to extract a separate spectrum for each spatial (x, y) point, as has been done for two points in Fig. 3.4. The visual appearance of the sample can be presented with a red–green–blue (RGB) image which is simulated from the spectral image [42].

3.4 PHOTOLUMINESCENCE

The incident EM radiation can also generate photoluminescence L in some subject materials, as seen in Fig. 3.5 (b), where a Norway spruce board emits yellowish and bluish light when excited with a UV–B [41] light source. In Fig. 3.5 (a) the same Norway spruce board is imaged under daylight illumination. Photoluminescence is a non–linear effect where a photon of incident radiation, with energy E = hc/λ, where h is Planck's constant and c is the speed of EM radiation in a vacuum, excites a material ion which is in a crystal lattice [47]. The excitation state will relax after some time and a new photon with energy E′ = hc/λ′ will be emitted. This

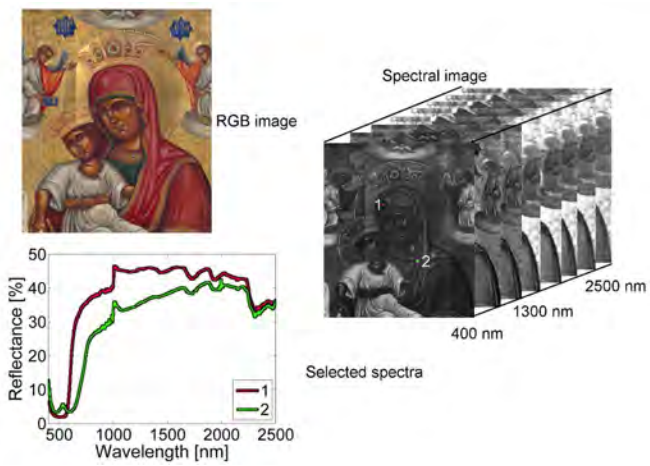

Figure 3.4: An example of a spectral reflectance image. Each gray scale image in the stack presents sample reflectance at a certain wavelength. Thus, each spatial (x, y) point has its own spectrum, as has been demonstrated for two points. An RGB image is simulated from the spectral image for visual preview.

new photon will have less energy than the original photon, i.e. $\lambda' > \lambda$ because a certain amount of energy will be lost in the crystal lattice. Photoluminescence can be divided according to excitation state lifetime into fluorescence (<10 ns) and phosphorescence (>10 ns).

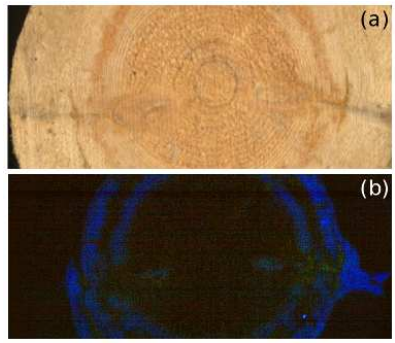

Figure 3.5: Photoluminescence of Norway spruce. An RGB image from a wood board (a) under daylight illumination and (b) under UV–B illumination.

A full examination of the photoluminescent properties of a subject material is obtained by exciting it one wavelength λ at a time and measuring the corresponding emission spectrum. The measurement is performed with a bispectrometric device which, in principle, consists of two monochromators, one for illumination and a second for detection [48]. However, in practice, to speed up the measurement process, the detection monochromator is often replaced with a spectrometer which is able to measure all wavelengths simultaneously. This procedure will produce the excitation–emission matrix as presented in Fig. 3.6. Spectral reflectance is located in the diagonal, where $\lambda = \lambda'$ and possible photoluminescence is below the diagonal, where $\lambda' > \lambda$. As a result, this procedure will produce a four–dimensional matrix L(x, y, λ, λ') for photoluminescence when repeated for every spatial point over the subject material surface. This measurement is a rather time–consuming process and produces a great deal of data when performed with small wavelength intervals. Hence, in this work only a UV–B light source is used for excitation, which means that just one horizontal line in Fig. 3.6 is measured as a function of the spatial domain.

Emission spectrum L(λ') can be obtained with an excitation light source, in which the SPD equals zero in the detection range as follows

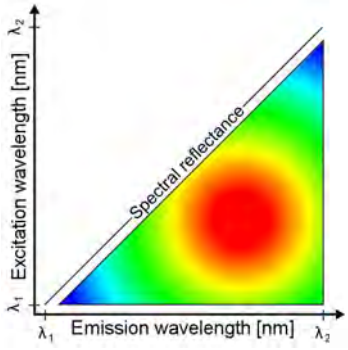

Figure 3.6: Excitation–emission matrix where spectral reflectance is in the diagonal and possible photoluminescence is below the diagonal.

$$L(\lambda') = \frac{S_S(\lambda') - S_D(\lambda)}{C(\lambda)}. \tag{3.3}$$

If the SPD of a light source does not equal zero in the detection range, the $L(\lambda')$ can be approximated using

$$L(\lambda') = \frac{S_S(\lambda') - S_R(\lambda)}{C(\lambda)}. \tag{3.4}$$

The latter method for $L(\lambda')$ extraction is not as accurate as the first, because the emitted and reflected signals could be mixed.

4 Adhesives and lumber

In this chapter the essential properties of the subject materials are introduced. Related measuring techniques are also reviewed and discussed.

4.1 ADHESIVES

Synthetic adhesives were introduced for wood gluing in the 1930s [25]. Adhesives have since been developed to be increasingly suitable for different kinds of end products and production lines. This can be seen in Table 4.1, where four common industrial adhesive types are presented with their key properties. Nowadays, some of these adhesives can produce joints that are strong as the wood, even when exposed to the weather.

Currently, the glued wood industry produces, for example, glulam boards, glulam beams, plywood and cross laminated elements. The service conditions of the end products also set requirements for adhesives which have to be fulfilled or a catastrophe could occur.

Table 4.1: Common industrial adhesive types and their key properties.

Property/adhesive	Polyvinyl	Polyurethane	Phenol	Melamine
Water–dilutable	x	Optional	x	x
Color	White	Transparent	Dark red	White
Heat curing	-	Optional	x	x
Catalyst	-	x	Optional	x
Solvent removal	Drying	Chemical	Drying	Chemical
Applications	Gluelam boards	Gluelam boards, plywood	Plywood	Plywood, gluelam beams

The proper use of these adhesives requires careful consideration of several variables, including temperature, moisture content, adhesive/catalyst ratio, assembling time, pressing time and amount of adhesive.

Adhesives are typically applied with several main coating techniques such as roll, blade, curtain, spray and extruder [25, 26]. At the moment, coating devices based on these techniques are advanced and moderately accurate. Thus, glued wood manufacturers significantly rely on these devices. However, there is usually no feedback system following the coating which notes the success of the process. It then depends on the coating device operator in regard to how rapidly malfunction and adhesive flow interruption can be recognized. Sometimes this issue is solved by slightly increasing the amount of applied adhesive, which does not actually solve the problem. Extra adhesive makes it difficult to get narrow joints and adhesive consumption is unnecessarily high and the amount and existence of the adhesive still cannot be verified. This challenge could be overcome with an appropriate device which is able to provide adhesive layer thickness information.

In recent years several methods have been studied and developed for thin film thickness measurement, as seen in Table 4.2. Of course, there exists also other measurement techniques (e.g. mechanical or electrical) but this work deals only with techniques which are based on photonics. Some methods (Table 4.2) apply interferometry, Raman scattering and ellipsometry but they are mainly suitable only for transparent films less than several microns thick. Moreover, most of these methods require the film to be in solid form. Existing reflectance–based methods for adhesive detection can verify the existence of an adhesive [28, 29]. Furthermore, in the case of stripe (also known as ribbon) coating these methods can approximate the amount of adhesive from the width of the stripe. Stripes of adhesive are extruded from equally spaced holes in a spreader pipe above a conveyor where glued parts are moving. The surface of the glued part is illuminated using a high angle from its surface normal and a camera is adjusted to look at the glued

Table 4.2: Overview for existing thin film measurement techniques and their key features.

Author	Method	Solution	Solid/ liquid	Wavelength range	Background	Thickness
William [28] (1956)	Diff./spec. reflection	Transparent solutions	Liquid	VIS	Various materials	–
Ruiz–Urbieta et al. [49] (1971)	Specular reflectance	Transparent films	Solid	633 nm	Absorbing substrate	1–4 μm
Azzam et al. [50] (1975)	Ellip–sometry	SiO_2	Solid	633 nm	Si substrate	108 nm<
Matsuda et al. [51] (1986)	Interfero–metry	Transparent polymers	Solid	633 nm	Frame support	1.4–2.7 μm
Edwards et al. [29] (1987)	Spec./diff. reflectance	–	Liquid	Polychro–matic	Paper materials	Existence
McCarty [52] (1987)	Raman scattering	Sodium sulfate	Solid	488 nm	PT/10 % Rh substrate	0–1 μm
May et al. [30] (1989)	Fluores–cence	–	Solid	UV	Various materials	–
Hutchinson et al. [53] (1995)	Raman scattering	Polyphenyl–ether	Liquid	633 nm	Diamond/ steel	0.1–10 μm
Gaon et al. [54] (2001)	Absorption	Water based	Liquid	1720–1900 nm	Carton	–
Amalvya et al. [55] (2001)	Speckle	White paints	Liquid	633 nm	Glass plate	75 μm, 150 μm
Taylor [56] (2002)	Absorption	Starch based	Liquid	1840/1940 nm	Paper	49 g/m^2
Mbachu et al. [26] (2005)	Absorption	Phenol–formaldeh.	Liquid	350–2500 nm	Wood	88–225 g/m^2
Mbachu et al. [57] (2005)	Absorption	Urea–formaldeh.	Liquid	400–2250 nm	Wood	0–12 % of mass
Otsuki et al. [58] (2005)	Ellip–sometry	Protein films	Solid	670 nm	Many layers	10–20 nm
Pristinski et al. [59] (2006)	Ellip–sometry	Polymetha–crylic acid	Liquid	633 nm	Si substrate	100 nm
Cowan et al. [60] (2007)	Absorption	Several adhesives	Liquid	1200–2400 nm	Wood	0–10 % of mass
Scarel et al. [61] (2010)	Optical phonons	Aluminium, zink oxide	Solid	2500–100000 nm	Si substrate	10–250 nm
Lauria et al. [62] (2012)	Absorption	Polyvinyl–acetate	Liquid	200–750 nm	Paper	0.1–2 mm

part from its surface normal direction. The camera observes the illuminated area due to the diffuse reflection of the glued part and specular reflection of the adhesive stripes cause darker lines in the image. The width of the adhesive line is strongly correlated with the amount of adhesive. Thus, the amount of adhesive can be estimated from the width of the line by multiplying it with a scale factor [27]. However, accurate adhesive film thickness cannot be resolved.

The fluorescence method is able to detect a film thickness within specific thickness range but it requires adhesives to be sufficiently fluorescent and this is not usually the case with all adhesives [30]. This could be solved by adding a fluorescent additive to the adhesive but it will increase costs and could decrease the strength properties of the adhesive. The target material to which the adhesive is applied should not be fluorescent or at least have a constant fluorescence.

The most promising solution has been offered by Mbachu and Congleton (2005) [26]. Their method applies partial least square regression to spectral data acquired over the 350–2500 nm wavelength range from a phenolformaldehyde adhesive on a wood surface. However, from a practical point of view their method has several disadvantages. Firstly, image data acquisition over a wide spectral range requires expensive sensors. Secondly, computation rapidly becomes cumbersome with high–dimensional data and real time implementation could be challenging. Hence, it can be concluded that an efficient solution is still lacking.

Table 4.1 indicates that all adhesives can be diluted with water. Thus, it could be possible to detect thicknesses of all these adhesive types if the amount of the water could somehow be measured. This approach could also provide an opportunity to extend the thickness detection method to other water–dilutable compounds, for example, paints, waxes, lacquers and wallpaper glues.

4.2 LUMBER

Lumber has been widely used by humans for different kinds of constructions and tools throughout history. Numerous properties of lumber have been studied and consequently it has been possible to use this knowledge for more challenging applications than ever before. One of the latest promising applications of lumber is an insulation panel which could replace non–renewable petroleum–based insulation materials [63]. Overall, biorefination of renewable feedstocks from biomass has become one of the key research fields

today and this will continue in the future [64, 65]. However, these processes are complicated and biomass pretreatments affect processing costs and efficiency.

Wood is an extremely complex organic structure and its appearance varies greatly among different species, individual trees, environmental conditions, processing methods and tools. This is the case in the Nordic wood production chain from forest through sawmill and end product packing. Depending on the season of the year, cut trees can be frozen or melted, which makes IR responses vary. The blades used for cutting and planing also produce wood surfaces with different roughnesses which affects scattering. Furthermore, the color of the wood varies within wood species and variations within some specific species can be also significant. Thus, it is recommendable to use wood samples which correspond to real conditions in wood production when developing machine vision methods and techniques. Because of these significant dependences, it should also be remembered that previously developed methods have also been studied under a number of conditions. Thus, these methods may not necessarily be directly applicable for other wood species and environments. Previous studies, however, offer an extensive framework for future work.

The spectral band assignments of wood and its components in near–infrared from the past 70 years have been collected by Schwanninger et al. (2011) and are presented in Fig. 4.1 [66]. These band assignments could be used as initial key wavelengths for the studies of two–dimensional mapping of compositions which is discussed in more detail later. Yeh et al. (2004) have also confirmed several of these assignments [17]. A similar comprehensive collection has been published by Elvidge (1990) from dry plant materials [67]. Soukupova et al. (2002) have studied lignin estimation from liquid samples and have also performed lignin related studies [68]. However, some attention should be paid in the analysis to overlapping spectral responses of the compositions, as seen in Fig. 4.1, because a strong separation of overlapping compositions could require the use of a complicated analysis [68].

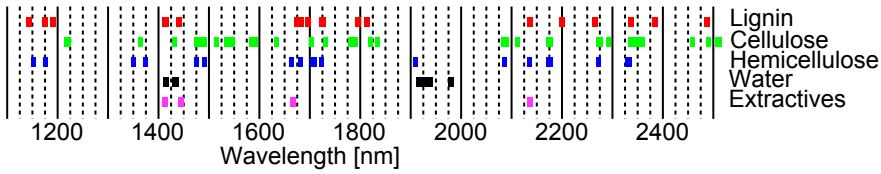

Figure 4.1: Near–infrared wavelengths associated with wood compositions, which could be used as initial key wavelengths for the studies of two–dimensional mapping of compositions. [66].

Existing MC detection studies of lumber have been collected by Leblon et al. (2013) [4]. An extension to their study is several similar studies which also apply near–IR techniques for MC estimation [23, 69,70]. An advantage of the near–IR technique over pin meters and computer tomography scanners is its ability to measure moisture and density independently [71]. However, it has also been found that changes of temperature in manufacturing environments affect near–IR response [71].

The majority of the previously introduced studies have operated with point–wise data acquired from a certain area. However, lumber is a heterogeneous material, which suggests that spatial distributions should be also taken into account [4]. Such two–dimensional mapping has been done for galactose, glucose and lignin [72], compression wood [7,31,32], moisture content and density [73]. In the future these novel visualizations of composition distributions could aid researchers in understanding wood material better.

In the previously introduced studies researchers have developed empirical models for optically obtained data from wood in order to determine one suitable for a given task. In contrast to this approach, Tsuchikawa et al. have studied a model for interaction between light and a wood material [74–76]. In these studies the structure of the wood has been simplified and considered to be an aggregate of semi–infinite long tracheids, as seen in Fig. 4.2. Surface roughness has been modeled with a uniform layer where the thickness is the maximum height of the surface roughness multiplied by a specific

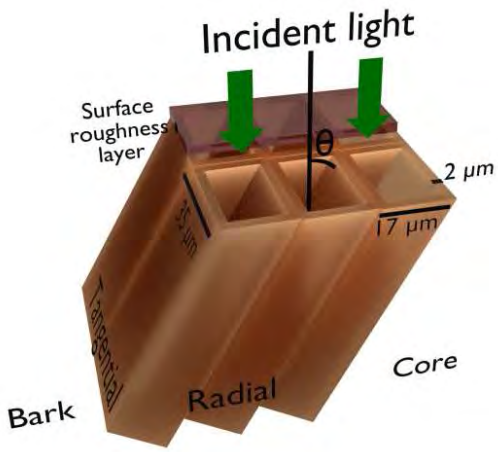

Figure 4.2: The simplified structure of wood for modeling interaction with light where wood is considered to be an aggregate of semi–infinite long tracheids. Surface roughness is modeled with a uniform layer where the thickness is the maximum height of the surface roughness multiplied by a specific constant. The dimensions correspond to late wood of Sitka spruce.

constant. The maximum height of the surface roughness has been obtained from a profile curve traced with a knife–edge type stylus. Data was measured point–wise from Sitka spruce (*Picea sitchensis*) samples with a integrating sphere. From this data the relationships between absorption and variables such as sample thickness, illumination angle, wavelength and surface roughness were examined.

It was determined that the Kubelka–Munk theory can be used to express the behavior of diffusely reflected near–infrared light from wood even though the Kubelka–Munk theory is generally related to the context of paper quality [77]. Three different bands (800–1400 nm, 1400–1860 nm, 1860–2500 nm) were distinguished according to scattering and absorption coefficients. However, the measuring setup used and the material under examination did not meet the assumptions of the Kubelka–Munk theory for diffuse illumination and an ideally scattering medium. Thus, these deviations from the ideal had to be compensated with a directional characteristics model, a light–path model and an equivalent surface rough-

ness model. Furthermore, the transmitted light case also requires the use of generalized input/output equations for radiation. These models have been supported by studies using different measuring techniques [78,79].

Nevertheless, these models are somewhat outside the scope of this work because they are meant more for the fine structure analysis of the wood material while the focus here is on the applications of spectral imaging. The measuring setups used are not directly applicable due to the different measuring geometry. However, one needs to be aware of these results because they could provide useful knowledge in the future when developing practical applications for wood material observation. This includes, for example, the fact that detection sensitivity could probably be increased with the proper measuring geometry for some feature or the effect of surface roughness could be reduced with appropriate wavelength band selection.

5 Materials and methods

This study is based on measurements done with the wide spectral range imaging system developed in Paper **I** for this purpose according to practical needs. This system is first presented and is then followed by the wood and adhesive sample preparation procedures used in Papers **II–III**.

5.1 HARDWARE CONFIGURATION

Line spectral camera–based imaging systems require scanning in at least one spatial domain to acquire a complete spectral image. Depending on the final spectral range even several line spectral cameras must be used and scanning repeated for every camera. Hence, the acquisition process could become time–consuming with a large sample set or even problematic with sensitive samples, for example, frozen ones. However, time consumption can be decreased using simultaneously operating line spectral cameras when only one scan might be enough. Such a solution has been developed in Paper **I** and presented in Fig. 5.1. The system consists of three line spectral cameras, operating in the UV (200–400 nm), VIS (400–1000 nm) and IR (1000–2500 nm) range of the EM spectrum. The efficiencies of spectrographs are $>$50 % and spectral resolutions are 2.0 nm, 2.8 nm, 10.0 nm for UV, VIS and IR respectively [80–82]. Average full width at half maximum values for UV, VIS and NIR are 3.7 nm, 3.2 nm and 10.7 nm respectively [83–85]. Cameras are attached in an aluminum profile frame and adjusted to observe the same line in target plane from a 0° angle. The view of the line spectral cameras located on the sides of the frame are reflected with silver surface mirrors. A sample is attached on the linear translation stage where the movement is perpendicular to the lines of the line spectral cameras. The EM radiation for the measurements is produced with UV–B and halogen light sources, which are placed on both sides

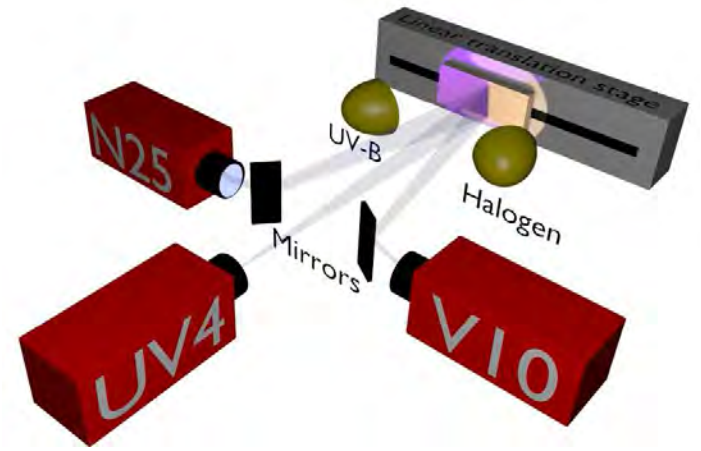

Figure 5.1: The setup of the wide spectral range imaging system. The line spectral cameras are adjusted to observe the same vertical line from the sample attached on the linear translation stage. Samples are illuminated by either UV–B or halogen light sources.

close to the sample at a 45° angle. Hence, realization of this system corresponds to 45°/0° geometry.

The line spectral cameras were adjusted so that the camera with the lowest spatial resolution was also able to discriminate majority of annual rings formed by early wood and late wood stripes from Scots pine. Annual rings have been reported to be associated with the density of wood which could be supportive information for the end users of the spectral image database [86]. This means a roughly dot size of 250 μm, which corresponds to a 80 mm field of view with 320 pixels. The line spectral cameras with higher spatial resolutions were also forced to this same resolution and the pixels which were otherwise cropped off were used for binning. Of course, higher spatial resolution would have been better because smaller details could have been observed, but it would have been a trade-off with measurement time, data size and sample set.

A custom–made graphical user interface (GUI) was developed and written in C++ programming language to control the line spectral cameras and the linear translation stage. The GUI allows the user to adjust the necessary acquisition parameters, for example,

exposure times, scanning length and step size.

The properties and features of the described system are presented in more detail in Paper **I**. The system has been used in the following sections of this work but also to measure icons, paper and wood chips. These religious icons (Fig. 3.4) have been painted with tempera on wood board (roughly size of 20 cm $\times$ 30 cm $\times$ 3 cm) in 18th century. In particular, icons contain invisible information in the IR range about painting technique or colorants used. On the other hand, icons are sensitive and extra cooling had to be implemented to manage the heat of the halogen lamp. Nor was it possible to perform UV imaging due to a photo bleaching effect which can damage icons.

5.2 SAMPLE PREPARATION

In total, 44 trees were harvested for wood samples in April 2011 from the Kajaani region of Finland, which is noted in Fig. 5.2 (a). Only the most economically significant wood species (birch, Norway spruce and Scots pine) in Finland were selected for inclusion in the database at this stage. Logs were cut in 25 mm thick boards and crosscuts with a band saw, as shown in Fig. 5.2 (b), in the wood laboratory of Cemis Oulu. After cutting, the samples were packed in plastic bags, transported to Joensuu and put in a freezer to await measurements. Before the measurements the samples were examined visually in order to select those which would produce as versatile a feature set as possible for the final database. In all, 36 crosscuts and 71 boards were selected for inclusion in the database. The measurements were carried out with the spectral imaging system presented in Paper **I** for frozen, melted and dried samples to make the data correspond to conditions in Finnish sawmills in different seasons. Sampling and preparation are described in more detail in Paper **II**. However, MC values 3.8–7.2 % reported in Paper **II** for dried samples are less than 40 % relative humidity (RH) would produce in room–drying [87]. RH was not constant in the laboratory during the year as assumed in the first stage. Reported

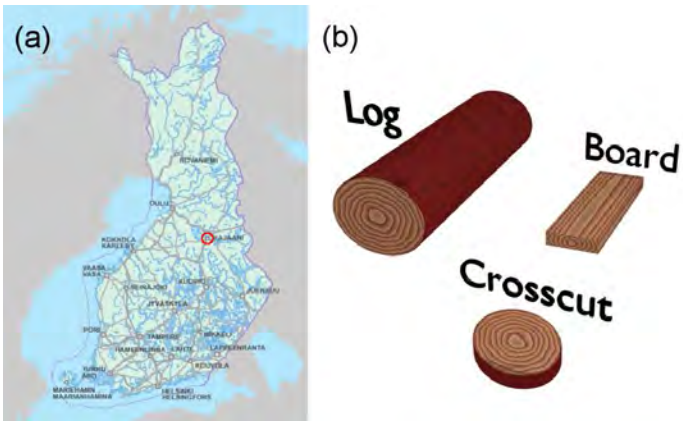

Figure 5.2: (a) Trees were harvested from the Kajaani region of Finland for the database. (b) Logs were cut to crosscut and board samples for spectral imaging.

40 % RH was measured during the performance tests of the spectral imaging system on October. Since that RH decreased even until 5 % during the spectral imaging process of wood samples which was performed from January to February.

The adhesives employed in Paper **III** were bought from a hardware store or obtained from an industrial partner. A total of six PV–based and one polyurethane–based adhesives were selected for the study. The recommended layer thicknesses for these adhesives were 0.1–0.3 mm according to the manufacturers. Hence, the method developed in the study should be able to operate within the 0–0.3 mm thickness range. Wood blocks, where solutions were applied, were obtained from the glulam board factory of an industrial partner. Wood blocks were cut from Scots pine boards and their equilibrium MC was approximately 12 %.

Adhesives were applied over wood blocks using the setup presented in Fig. 5.3 because an appropriate reference method could not be found for layer thickness verification. A metal piece with a known thickness d is attached in one edge of the wood block with screws. Then a slightly excessive amount of adhesive is applied to the wood block next to the metal piece. Finally, the extra adhesive is wiped away with a straightedge resting on the corners of the metal

piece and the wood block. The straight line (dashed line in Fig. 5.3) z(x) along the adhesive surface with a constant y–value then corresponds to the adhesive thickness. According to the selected coordinate system, z(x) can be expressed as follows:

$$z(x) = \frac{z(x_1)}{x_1} \cdot x, \tag{5.1}$$

where $z(x_1) = d$.

It should be noted that this application method only functions for reference use for solutions with reasonable viscosity. Solutions with too low a viscosity are not able to maintain the formed linear thickness distribution. Here viscosity was visually approximated to meet this requirement for all solutions used. The wood blocks with applied adhesives were then measured with the spectral imaging system presented in Paper **I**.

Paper **III** deals only with adhesives, even though it was assumed that the developed method should also be operational for other water–dilutable solutions. Thus, the six additional water–dilutable solutions listed in Table 5.1 were tested with the method developed in this study.

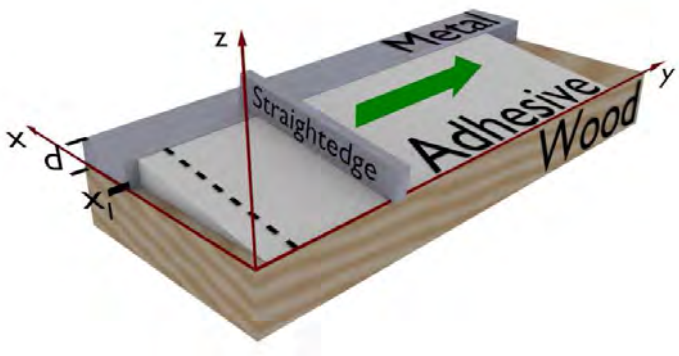

Figure 5.3: The setup for applying the adhesive layer with a known thickness. Extra adhesive is wiped away by gliding a straightedge, which rests on the corners of the metal and wood, from left to right.

Table 5.1: Recommended layer thicknesses for solutions used in this work.

Solution	Type	Thickness [mm]
Siro	Priming paint	0.09–0.20
Liberon	Panel wax	0.08
Pride	Wallpaper glue	0.13–0.17
Kiva	Furniture lacquer	0.07–0.13
Melamine†	Industrial adhesive	Unknown
Hardener†	Industrial hardener	Unknown

† Solutions from Akzo Nobel Finland Oy.

6 Results

In this chapter, the summarized results of the spectral imaging system performance tests are presented. This is followed by the introduction of the spectral image database of Nordic sawn timbers and its potential. Finally, the method developed for adhesive thickness measurements is discussed.

6.1 SPECTRAL IMAGING BENCHMARK

The wide spectral imaging system developed here consists of many parts with a partial effect on overall accuracy and performance. It is crucial to know the operational ranges and possible limitations for proper use and valid data. In Paper **I** the system is benchmarked with a peak signal to noise ratio (PSNR), spatial resolution and spectral accuracy.

In Paper **I** PSNR is presented as a function of wavelength. It was found that PSNR exceeds 30 dB in the 297-350 nm, 368-370 nm and 400-2488 nm ranges and 35 dB in the 309-331 nm and 400-2425 nm ranges. Gaps in the PNSR values originate from the SPDs of light sources and the responses of sensors, in other words, from the dynamic range of the imaging system which is discussed more later. According to the equation 4 of Paper **I**, the PSNR values 30 dB and 35 dB mean that the amount of noise in the signal is 3.2 % and 1.8 % respectively, unlike what has been explained in Paper **I**. Effect of PSNR is demonstrated in Fig. 6.1 for dark corrected signal with the 95 % confidence intervals of 35 dB and 20 dB PSNR. The 95 % confidence interval means that 95 % from new observations would fall inside this interval [88]. In Fig. 6.2 the effect of PSNR is demonstrated for a homogeneously colored and lit surface and a real image where images are contaminated with noise which corresponds to different PSNR.

Based on visual observation of Fig. 6.1 and Fig. 6.2 it can be con-

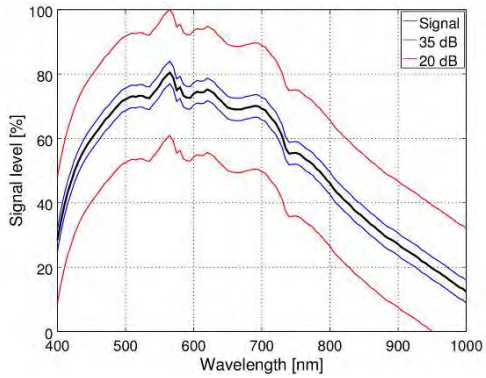

Figure 6.1: Demonstration of PSNR for dark corrected signal. 95 % confidence intervals are drawn with blue for 35 dB PSNR and with red for 20 dB PSNR.

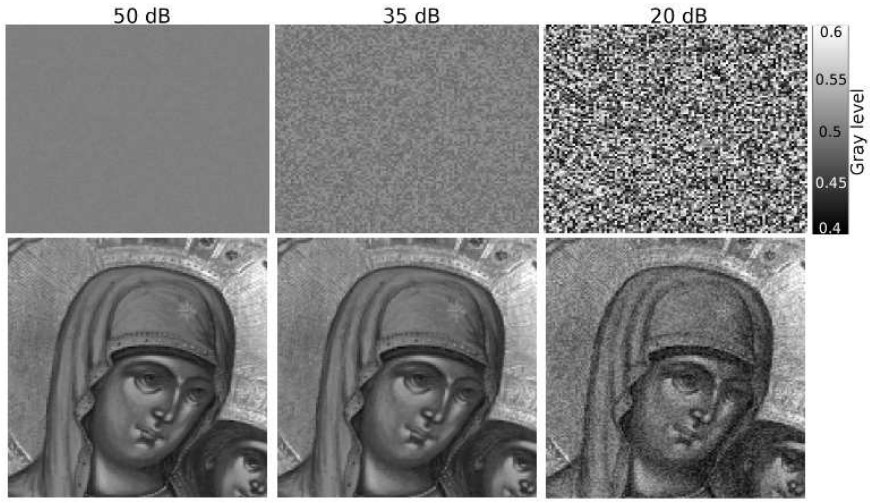

Figure 6.2: Demonstration of PSNR for solid and real image. Images in the columns are contaminated with noise which corresponds 50 dB, 35 dB and 20 dB PSNR.

cluded that previously introduced PSNR level of 35 dB seems to be tolerable. However, it is hard to draw any strict limit for acceptable PSNR because a limit depends on the task that is required. Tasks where spectra differ clearly from each other can tolerate more noise than tasks where spectra are nearly similar, because small crucial details may be hidden by noise. Noise could be also be decreased

with different post–processing algorithms, for example, Gaussian smoothing and non–local means algorithm [89].

Noise originates from several sources such as transfer noise, dark current, fixed pattern noise, high energy radiation, thermal noise, shot noise, analog–to–digital conversion and electrical interference. All of these may affect the output signal with different magnitude. Sensor manufacturer has presumably solved some of these problems but still it is good to be aware of the noise sources. Thus, this work does not just concentrate on noise, which is an extensive topic, in more detail. However, in this study dark current and fixed pattern noise have been taken into account according to equation 3.1 and the magnitude of overall noise has been examined as a function of wavelength. [42]

PSNR actually describes the quantification constancy of the system more than the accuracy. An improved visualization of quantification accuracy than that provided by PSNR is demonstrated in Fig. 6.3, where the dynamic range is plotted as a function of wavelength. Fig. 6.3 indicates that effective dynamic range, as well as quantification accuracy, is only 10 % of the maximum at both edges of the operational wavelength range. This relatively notable variation is not so critical if the bit depth of a sensor is sufficiently large.

Spatial resolution is an essential property for imaging devices

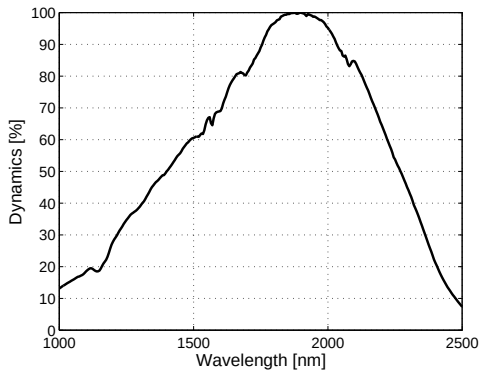

Figure 6.3: Dynamics of the spectral imaging system as a function of wavelength in the IR region.

and can be suitably investigated with a resolution target, for example, USAF–1951, as was the case in Paper **I** and in Fig. 6.4 (a). The spatial resolution readings in Paper **I** are also presented in Table 6.1, where different criteria for reading spatial resolution values have been compared. Table 6.1 demonstrates that in the developed system there are differences in spatial resolution between wavelength ranges. Differences also exist between the horizontal and vertical directions across the spatial domain. The horizontal direction is the same as the scan direction of the linear translation stage and has a lower spatial resolution. This originates from the width of the scan line in the scan direction, which is greater than the distance between the acquisition positions. In this case, the line under acquisition slightly overlaps with the previous and following lines. Unfortunately, the distance between the acquisition positions cannot be increased to eliminate overlapping because it would change the aspect ratio of the final image and the pixels would no longer be square. One solution could be the use of narrower slits in the cameras, but that would require changes from camera manufacturers.

It was found that the visual extraction of resolution target readings can be a subjective task. According to basic workflow, the user looks for the smallest line pair (LP) pattern in the image where the lines can still be separated. The corresponding resolution value is then obtained from a table according to pattern number. The task becomes subjective close to the resolution maximum, where the gray level changes are small and the line separation is the most challenging. Visual observation provides an approximate value depending on the observer and circumstances, when it is not necessarily sufficiently consistent for scientific purposes. More consistent results can be achieved with contrast criteria such as Rayleigh or Sparrow [90]. The Rayleigh criterion requires a 26.5 % drop in contrast while the Sparrow criterion makes it possible to separate objects with a zero contrast difference. This is possible when the outline pattern of two point sources has a small dip. However, resolution targets have dark and white bars instead of a pattern

produced by point sources and Sparrow's criterion is not suitable.

An alternative criterion is suggested here and can be derived from the noise of the imaging system. The idea is based on the recommendation of Willard et al. (1988) that the signal magnitude should be three times higher than the standard deviation (STD) of the noise [91]. First, the gray levels of the resolution target line [in Fig. 6.4 (a)] are plotted as a function of location, as shown in Fig. 6.4 (c). The STD of the noise of the image is then estimated from a uniform area, as shown in the green rectangle in Fig. 6.4 (a). The cyan decision lines in Fig. 6.4 (c) are then calculated with $\pm 1.5 \cdot$STD of the noise and plotted in the first figure, as shown in Fig. 6.4 (c). The offset of the decision lines should be adjusted according to the smallest pattern by adding a suitable constant. At this point, the user looks for the smallest pattern where the dark and white

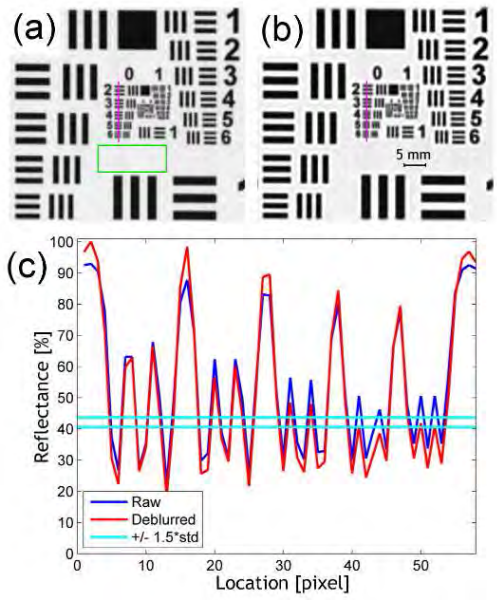

Figure 6.4: The resolution target at 550 nm in (a) in raw format and (b) deblurred with the point spread function. (c) The reflectances of the magenta sample lines, from top down, from (a) and (b) as a function of location. Cyan lines are $\pm 1.5 \cdot$STD of noise, which is estimated from the area of the green rectangle in (a).

parts still break decision lines. The advantages of the proposed method is that effect of the noise is taken into account and visual–decision making is easier with plotted lines than directly from the gray image.

The comparison between the criteria for reading spatial resolutions can be seen in Table 6.1. The compared criteria are the visual (Paper **I**), Rayleigh and previously suggested noise–based approach. Table 6.1 indicates that the visually obtained readings are similar or slightly higher than those obtained with the Rayleigh and noise–based criteria. The only exception was obtained with the noise–based criterion in the 1000-2500 nm range with a 2.00 LP/mm reading. This is actually the theoretical maximum for the setup of the developed system because it corresponds to the Nyquist frequency with a 250 μm dot size [92].

However, resolutions can be improved with post–processing, for example, deblurring or sharpening, as has been demonstrated in Fig. 6.4 (b) with the symmetrical point spread function (PSF). Fig. 6.4 (c) shows that PSF deblurring increases readings for white parts and decreases them for dark ones. Table 6.1, however, suggests the use of an anti–symmetric PSF to obtain improved deblurring results.

Table 6.1: Comparison of criteria for reading spatial resolution values. Paper **I** *values are obtained visually, Rayleigh values with a 26.5 % contrast difference and suggested values exceeding 3·STD of the noise level. Readings are in [LP/mm] unit.*

Orientation	Criterion	Wavelength range [nm]		
		200–399	400-999	1000-2500
Horizontal	Paper **I**	1.00	1.00	1.78
	Rayleigh	1<	1<	1.78
	Suggested	1<	1<	2.00
Vertical	Paper **I**	1.78	1.41	1.26
	Rayleigh	1.78	1.26	1<
	Suggested	1.78	1.26	1.26

The spectral accuracy of the system was verified with reference measurements. A PerkinElmer Lambda 1050 spectrophotometer was used to measure 22 non–fluorescent GretagMacbeth ColorChecker patches for reflectance verification. The luminescence case was examined with six Fluorilon^{TM}patches, which were excited with a UV–B light source. The spectrum of the UV–B light source was measured with a Hamamatsu PMA11 C7473 spectrometer and used to simulate the emission of luminescent samples from the reference data. The results of these measurements are presented in Fig. 4–5 of Paper **I** and indicate that the spectra do not perfectly overlap even though the degree of error is small. The rising edge of the luminescent spectra follow accurately while the falling edge has a tail, which results in greater error. However, this error is smaller for samples which are having emission maximum at longer wavelengths. The reason for this behavior is unclear. Reflectance spectra also follow each other although the devices have different measuring geometries. The largest error can be found in the wavelength range extremities of the sensors where previously discussed effective dynamic range and PSNR are lowest. The examination was only performed visually from graphs since it would not be reasonable to numerically evaluate error (e.g. root mean square error and color difference) between devices with different measuring geometries.

6.2 SPECTRAL IMAGE DATABASE OF LUMBER

The obtained measurements produced the database presented in Paper **II**, which contains approximately 44 million spectra. Half of the database contains reflectance data and the other half photoluminescence data. The surface features of each sample were observed visually and listed in a separate file for rapid access. The database requires 70 GiB of disk space in corrected format and 447 GiB in raw format.

The correct format of the database, i.e. the extracted reflectance and photoluminescence, was obtained by making all necessary com-

putations as described in Chapter 3 and Paper **I**. The data was also resampled with spline interpolation for 5 nm equal intervals for more convenient future use. The spectral images from the different sensors were then registered to remove a small position mismatch due to the setup geometry. The image registration was performed with an automatic generalized dual bootstrap iterative closest point algorithm [93, 94]. Hard images, where the automatic algorithm failed, were registered with a commercial software package (MATLAB 2012a, The MathWorks Inc., USA) with manually selected control points.

No further processing, for example, commonly used multiplicative scatter correction or derivatives extracted with numerical differentiation as reviewed by Rinnan (2009) [95], was performed for the database. The purpose of these processing methods is to improve regression, the classification model or exploratory analysis. These methods, however, have adjustable parameters which will affect the final result when crucial information for some specific application might be lost with static parameter selection. Hence, end users are encouraged to perform the required processing themselves to avoid possible information loss which could limit the use of the database. However, use of the first and the second derivatives have been demonstrated for lignin distribution extraction later in this section and in Paper **II**.

The database was introduced in Paper **II** and the public web page was created as a distribution channel. In Paper **II** the potential and possibilities of the database were demonstrated with one photoluminescence and two near–infrared examples. In the photoluminescence example the spatial distribution of the decay process was presented and the similar spatial distribution visualization of heartwood/sapwood is shown in Fig. 6.5. From the top of Fig. 6.5 (b) a lighter heartwood region which emits more photoluminescent light than the darker sapwood region below can be clearly distinguished. This distribution is presented more accurately in Fig. 6.5 (c), where the magnitude of the photoluminescence from one column of Fig. 6.5 (b) is plotted as a function location.

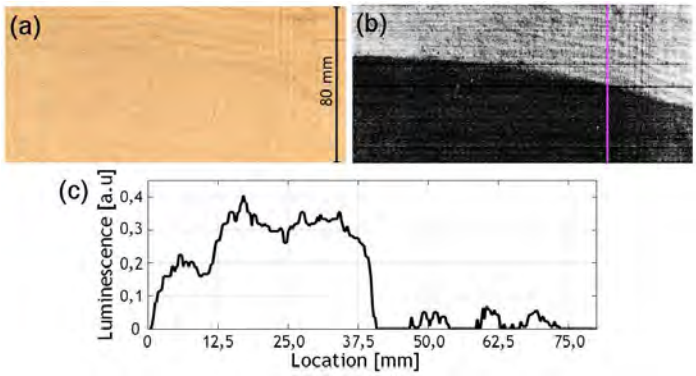

Figure 6.5: The spatial distribution of the heartwood/sapwood of Scots pine revealed by photoluminescence. (a) The simulated RGB image of the specimen under D65 illumination. (b) The photoluminescence of the specimen at 430 nm excited by a UV–B light source. (c) The magnitude of photoluminescence as a function of location along the magenta sample line (up to down) from (b). Magnitude of photoluminescence varies spatially (c) and the greatest level difference is between heartwood and sapwood (b). This suggests that photoluminescence could be used to distinguish heartwood from sapwood.

The first IR application example in Paper **II** was the spatial distribution study of aromatic lignin from frozen, melted and dried Norway spruce; it relates to the field of chemical mapping [96]. The first derivatives were calculated at 1675 nm and the obtained distributions were identical despite the state of the specimen. A similar lignin distribution example is presented in Fig. 6.6 (b), where the second derivative at 1675 nm is calculated for Scots pine board. In Fig. 6.6 (c) the second derivatives for heartwood and sapwood samples in Fig. 6.6 (a) are plotted with the key wavelengths of lignin according to [66]. The second derivatives were obtained with the gap–segment method, where the size of a differentiation window can be adjusted [97]. Adjustable window size allows the user to extract different latent features from the original signal. Fig. 6.6 (c) demonstrates that the second derivatives of heartwood and sapwood overlap and separate many times across the wavelength region. For example, the difference at 1675 nm will produce a pseudo color image, as visualized in Fig. 6.6 (b). However, all lignin–associated wavelengths do not produce similar a contrast between

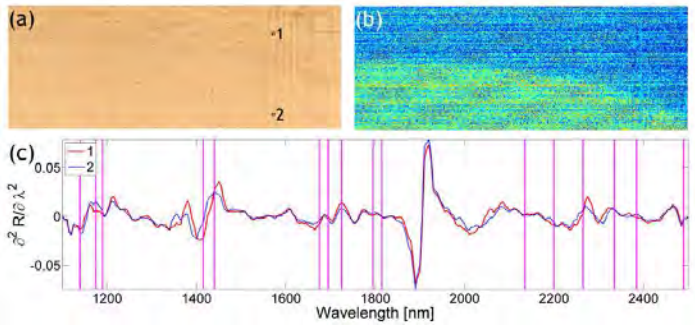

Figure 6.6: The spatial distribution of the lignin of Scots pine board revealed in the near–infrared part of the EM spectrum. (a) The simulated RGB image of the specimen under D65 illumination. (b) The second derivative at 1675 nm. (c) The second derivatives of two samples from (a) and lignin–associated wavelengths marked with vertical magenta lines.

heartwood and sapwood, as can be seen in Fig. 6.6 (c). Fig. 6.6 (b) seems to be quite noisy which originates from the small differentiation window of the gap–segment method. Image quality could be improved with wider differentiation window or with more sophisticated differentiation algorithms, for example, Norris–Williams and Savitzky–Golay [95].

The second IR example of Paper **II** was a practical method for the MC prediction of lumber. The average ratio $R_{1935\text{ nm}}/R_{1850\text{ nm}}$ was calculated for each sample spatially and compared with the known MC, as seen in Fig. 3 of Paper **II**. A linear trend was determined for each wood species separately even though the variation of some specimens exceeded standard deviation limits. The variation originates from the heterogeneous MC distributions of the samples and the sizes of samples greater than the imaged area. The method was found to be suitable only for fresh melted lumber. With frozen and dried lumber the data points more or less scattered without forming any clear trend.

6.3 ADHESIVE MEASURING METHOD

It was found at the beginning of Paper **III** that the reflectance of water–dilutable compounds was proportional to layer thickness in the near–infrared region. The proportion was non–linear, as expected according to section 3.2. Instead of using the whole spectrum, only two wavelengths (1445 nm and 1295 nm) were selected for further analysis. The first wavelength was strongly absorbed by water and hereby its reflectance was proportional to layer thickness of water–dilutable compounds. The second wavelength was highly transmitted through water and thus having a low response for water. Hence, the first wavelength was for observation purposes while the second was used as a reference. The ratio $r = R_{1445\ nm}/R_{1295\ nm}$ was calculated and used in the calculations. The use of the ratio is advantageous because it normalizes possible variations in measurement, for example, fluctuation and geometrical distortion.

The Lambert–Beer law was found suitable for layer thicknesses less than 0.04 mm, which is less than the recommended thicknesses (Table 5.1). This derives from the relatively high attenuation coefficients of the compounds used. Thus, the Lambert–Beer–based model was found to be inappropriate for this task. For the extended thickness range an empirical third–order polynomial model was developed. This model allowed thicknesses to be measured up to 0.15–0.5 mm, which was sufficient according to consumption recommendations. At higher thickness values accurate measurement is not possible, but the existence of an adhesive can still be verified.

In Paper **III** adhesive–dependent modeling parameters and test results were presented. They are similar to those presented in Table 6.2 for compounds studied in this work. The Pearson's correlation coefficient obtained was higher than 0.81 for all compounds [88]. The achieved mean accuracy was $\pm$ 0.02 mm while the minimum was $\pm$ 0.07 mm in the 0–0.25 mm thickness range. The mean accuracy corresponds to 8 % error from the maximum layer thickness which is a reasonable result. Similarly, the minimum accuracy corresponds to a 28 % error which might seem poor but it must

Table 6.2: The modeling parameters for Equation 1 of Paper **III** *for measured solutions. Modeling and testing accuracy in R^2, mean error and maximum error in mm units.*

Solution	a	b	c	d	$R^2_{modeling}$	R^2_{test}	Mean error [mm]	Maximum error [mm]
Siro[†]	-163.1	322.6	-212.6	46.8	0.87	0.87	0.02	0.06
Liberon[††]	-415.7	743.2	-441.2	87.0	0.85	0.85	0.01	0.04
Pride	-16.5	17.1	-5.7	0.7	0.95	0.96	0.02	0.06
Kiva	-8.6	12.9	-6.6	1.2	0.89	0.95	0.03	0.07
Melamine	-4.3	7.7	-5.2	1.4	0.99	0.99	0.01	0.05
Hardener	-14.0	19.5	-9.5	1.7	0.99	0.98	0.01	0.05

Thickness range [†] 0–0.2 mm [††] 0–0.15 mm.

be kept in mind that these values originate only from a few data points. Hence, mean accuracy describes overall performance better even though the maximum inaccuracy is good to be acknowledged. The accuracy of the method is also demonstrated in Fig. 6.7, where predicted thicknesses are plotted as a function of real thickness. A variation similar to oscillation can be seen for Kiva, in particular, and originates from the early wood/late wood stripes of the wood block as seen in Fig. 6.8. Other solutions are not as transparent as Kiva, thus the effect of background material is weaker. However, ideal background material would be observed to be homogeneous as discussed in Paper **III**.

Information concerning determined thickness can be visualized in several ways and one possibility is presented in Fig. 6.9, where thickness distribution is presented as a two–dimensional map. Fig. 6.9 also shows the effect of adhesive drying during image acquisition because thickness values are lower on right–hand than the left–hand side despite the same initial thickness. Hence, it was predicted that the developed method could be applied to drying process monitoring in the same way as a speckle method [55]. For this purpose ratio r is observed as a function of time.

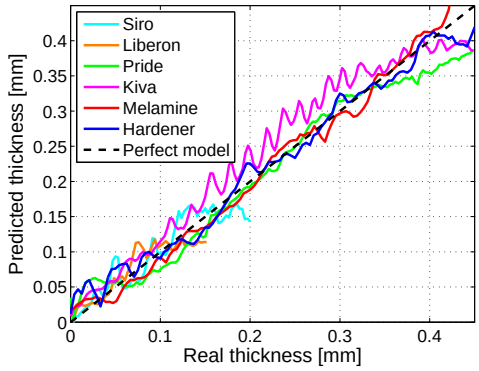

Figure 6.7: The accuracy of thickness prediction models as a function of real thickness for different solutions.

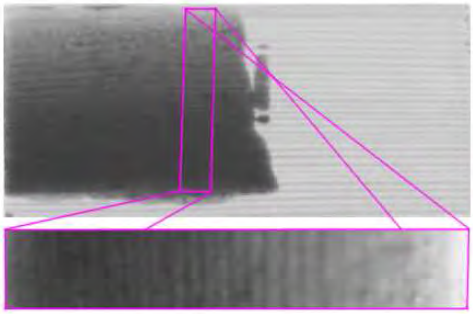

Figure 6.8: The image of the ratio r for the Kiva solution. Early wood/late wood stripes of the wood block are distinguished behind the Kiva solution and causing oscillation stylish variation in thickness prediction results (Fig. 6.7).

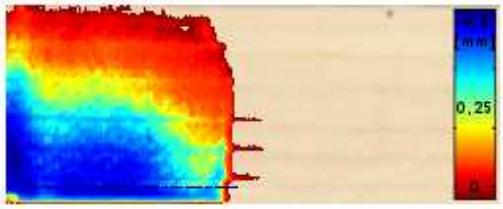

Figure 6.9: Two–dimensional thickness map obtained with the developed method for freshly applied PV adhesive.

7 Discussion

In this chapter the obtained results are considered against the aims of the work and discussed in detail.

7.1 SPECTRAL IMAGING SYSTEM

The wide spectral range imaging system developed in this work was the first reported with such a wide spectral operation range and the ability to measure photoluminescence according to the literature review done in Paper **I**. The absence of existing systems required substantial effort to develop a custom system from devices available in the laboratory. During the development process different options were considered and tested which led to the final configuration. The performance of the system was investigated using different benchmarks and attention should be paid in the future to these boundaries when working with the system.

PSNR and effective dynamic range were found to be satisfactory in the middle of the spectral range of each camera. Both values decreased towards the edges of the operational ranges, reducing accuracy. This resulted in a mismatch between spectra at the fusion point where the cameras change. One possible solution to compensate for the decrease in PSNR and effective dynamic range towards the edges could be a light source with a U–shaped SPD. This could be achieved with a programmable light source or by manipulating the SPD of the existing light source with suitable light emitting diodes or a transmission filter. However, halogen lamps already have their own emission maximum at about 1000 nm, where the VIS and IR cameras change according to Wien's displacement law [98, 99]. Hence, an even greater increment of spectral power in this region could lead to irreversible processes in samples without any appropriate cooling.

Spatial resolution was found to vary between the cameras used

which is natural due to their different optics. Variation in spatial resolution also occurs between spatial domains. Especially in the scan direction, the lines slightly overlap and blur the final image. The obtained spatial resolutions were roughly half the theoretical maximum but still enough to separate the majority of the annual rings of Scots pine which was the aim. Nevertheless, this can be improved slightly with post–processing, for example, deblurring and sharpening. The best results could probably be obtained by measuring PSF for each camera and employing it with appropriate deblurring algorithm to fix the final images [100].

The spectral performance of the system was investigated by comparing results with a reference device. The results were satisfactorily similar inside the high PSNR and effective dynamic range regions despite the different measuring geometries of the devices. The effect of different measuring geometry becomes more significant the less diffuse the samples and white reference are because specular reflection begins to occur. The degree of diffusion could be verified with goniometric measurements.

The UV region of the EM spectrum was found to be more challenging for imaging compared to the VIS and IR regions. The signal quality usually obtained is lower due to 1) the lower reflectance of most samples, 2) the lower spectral power of the light source and 3) the lower response of the sensors. Moreover, the reflectance and photoluminescence signals are mixed and strong separation requires the use of two monochromators. Furthermore, the illumination power cannot be increased too much or the samples could be contaminated due to the photobleaching effect. In this study the UV–B light source used for illumination does not cover the full detection range. Gaps in the spectrum could be filled with suitable light emitting diodes and this solution could also provide more accurate reflectance and photoluminescence separation. This is because individually controlled light emitting diodes could act as a second monochromator. A second solution could be to replace the UV–B light source with a supercontinuum light source, which can provide a relatively flat SPD over the operational range. However,

despite the challenges, the UV region can offer substantial information about the object under examination, especially if the spatial distributions of the properties can be resolved.

7.2 SPECTRAL DATABASE

The spectral image database of lumber measured in this work was obtained from the three most economically significant wood species in Finland. Attention was paid to sample handling and feature selection in order to obtain extensive and representative data. The amount of different species in the study was a compromise between sample amounts within available resources. However, the database could be later extended with different wood species and additional samples.

The spectral image data obtained consist of reflectance in the UV–VIS–IR range of the EM spectrum, which contains a considerable amount of information about the sample state and quality. For example, from this data it is possible to observe the spatial distributions of aromatic lignin and heartwood/sapwood as it has been demonstrated in this work and in Paper **II**. Moreover, the photoluminescence excited by the UV–B light source was also obtained. Even though the photoluminescence data was obtained only with one excitation, it still offers a totally different method for use in lumber quality studies. Accurate bispectrometric measurement would have been the best solution for determining the photoluminescent properties of lumber, but it would have been a trade–off with measurement time, data size and sample set.

The features of the samples, for example, knots and decay, were observed visually and listed in binary tables for convenient future use. No chemical analysis was performed on the samples during the measurement. However, they can still be performed because the dried samples have been stored. Spatial binary masks for different features could also be developed for faster data access. Binary masks would be a convenient solution due to their small storage space requirements. This would allow sharing between researchers

via the web; for example, the developed masks could be maintained with the web pages created for the database.

The potential of imaging spectroscopy for lumber studies was demonstrated with a number of examples. The main advantage of the imaging technique is that it allows the study of the spatial distributions of the features under examination as it has been introduced in previous studies [4, 31, 72, 73]. On the other hand, it also rapidly produces huge amounts of data, which is a sound basis for statistical analysis. Demonstrations revealed interesting connections between reflectance and the photoluminescent responses of lumber, especially for lignin, which was also associated with heartwood and sapwood. The database was also applied to develop a practical method for the MC estimation of lumber. A linear trend between the predicted and real MC was determined even though the remaining standard deviation could not be ignored. However, accuracy could be improved with additional measurements of homogeneous samples.

7.3 ADHESIVE APPLICATION

Two wavelengths from the IR range used were found to be responsive to the layer thickness of water–dilutable compounds. The IR range of the EM spectrum also offered reference wavelengths for data normalization. These discovered wavelengths were then used to develop a practical method for layer thickness measurement. Even though the method was developed with image data, it can also be scaled down for a line or a spot.

The Lambert–Beer law was found to be limited to layer thickness measurement within the thickness recommendations of compound manufacturers. Thus, an empirical third–order polynomial model was developed to obtain the required dynamic range for the measurement. The Lambert–Beer law could probably also have been customized using external terms to obtain a greater thickness range, but this was not tested because the empirical model was already seen to be appropriate.

The method was also successfully extended from adhesives to other compounds due to their common diluter, water. This increases the number of possible applications in the wood industry, from glued wood production to all–over surface finishing. Furthermore, the method could be applied for other background materials than wood, if the determined requirements for a background material are fulfilled.

The main advantage of the method from a practical point of view is that it requires only two wavelengths to be observed. Hence, the sensors used could be simple and low–cost compared to hyper–spectral ones and computation would be simple due to the small dimensional data, which is a solid basis for real–time processing. These are important features when searching for a high–throughput production line implementation.

The ability to measure wet compounds is a great benefit compared to the techniques employed for dry ones. Wet measurement allows the repair of faulty parts or their rejection from the process, which could save production resources. The method was also found to be applicable to drying process monitoring because drying is the loss of water in the compounds used and this affects to the absorption of near–infrared radiation. On the other hand, this sets a constant water concentration requirement for the compounds used.

8 Conclusion

In this work a wide spectral range imaging system with photoluminescence imaging ability has been introduced. The developed setup can be widely customized for different measuring geometries and spatial resolutions. The system was benchmarked with different tests in order to obtain knowledge about performance and the appropriate operational range. The most significant challenges were found in the UV region of the EM spectrum due to several reasons. However, the UV region could hold a great deal of information about the samples under examination, which suggests directing more effort towards the challenges of UV range imaging in the future.

The wide spectral range imaging system was applied to two research cases in the context of the wood industry. The first research case was the acquisition of a public spectral image database of sawn timber for research purposes. Sample handling and selection were to be performed so that the final database would correspond to data from real sawmill conditions and be as versatile as possible. As a result, the final database contains approximately 44 million spectra, which connect spectral information over the UV–VIS–IR range pixel–wise. According to the performed analysis it was confirmed that the database provides possibility to access the spatial distributions of wood properties and compounds.

The second research case was the development of a practical method for adhesive layer thickness measurement. Key wavelengths associated with layer thickness were determined and used to derive a model which requires the monitoring of only two wavelengths. Furthermore, the key wavelengths were the absorption peaks of water, which allowed the extension of the method to other water–diluted compounds as well. This feature offers considerable possibilities for the method because nowadays water is a common diluter in industrial and surface finishing compounds.

Bibliography

[1] J. Antikainen, T. Hirvonen, J. Kinnunen, and M. Hauta-Kasari, "Heartwood detection for Scotch pine by fluorescence image analysis," *Holzforschung* **66,** 877–881 (2012).

[2] M. Vilaseca, B. Schael, X. Delpueyo, E. Chorro, E. Perales, T. Hirvonen, and J. Pujol, "Repeatability, reproducibility, and accuracy of a novel pushbroom hyperspectral system," *Color Research & Application* (2013).

[3] S. Tsuchikawa, "A review of recent near infrared research for wood and paper," *Applied Spectroscopy Reviews* **42,** 43–71 (2007).

[4] B. Leblon, O. Adedipe, G. Hans, A. Haddadi, S. Tsuchikawa, J. Burger, R. Stirling, Z. Pirouz, K. Groves, J. Nader, and A. LaRocque, "A review of near-infrared spectroscopy for monitoring moisture content and density of solid wood," *The Forestry Chronicle* **89,** 595–606 (2013).

[5] O. Hagman, *On reflections of wood: wood quality features modelled by means of multivariate image projections to latent structures in multispectral images*, PhD thesis (Luleå University of Technology, Skellefteå, Sweden, 1996).

[6] H. Kauppinen, *Development of a color machine vision method for wood surface inspection*, PhD thesis (University of Oulu, Oulu, Finland, 1999).

[7] P. Duncker and H. Spiecker, "Detection and classification of Norway spruce compression wood in reflected light by means of hyperspectral image analysis," *IAWA Journal* **30,** 59–70 (2009).

[8] P. K. Lebow, C. C. Brunner, A. G. Maristany, and D. A. Butler, "Classification of wood surface features by spectral reflectance," *Wood and Fiber Science* **28,** 74–90 (1996).

[9] S. Tsuchikawa, K. Inoue, J. Noma, and K. Hayashi, "Application of near-infrared spectroscopy to wood discrimination," *Journal of Wood Science* **49,** 29–35 (2003).

[10] K. Pandey and A. Pitman, "FTIR studies of the changes in wood chemistry following decay by brown-rot and white-rot fungi," *International Biodeterioration & Biodegradation* **52,** 151–160 (2003).

[11] B. Mohebby, "Attenuated total reflection infrared spectroscopy of white-rot decayed beech wood," *International Biodeterioration & Biodegradation* **55,** 247–251 (2005).

[12] A. Naumann, M. Navarro-González, S. Peddireddi, U. Kües, and A. Polle, "Fourier transform infrared microscopy and imaging: Detection of fungi in wood," *Fungal Genetics and Biology* **42,** 829–835 (2005).

[13] B. K. Via, C.-L. So, L. G. Eckhardt, T. F. Shupe, L. H. Groom, and M. Stine, "Response of near infrared diffuse reflectance spectra to blue stain and wood age," *Journal of Near Infrared Spectroscopy* **16,** 71–74 (2008).

[14] J. B. Hauksson, G. Bergqvist, U. Bergsten, M. Sjöström, and U. Edlund, "Prediction of basic wood properties for Norway spruce. Interpretation of near infrared spectroscopy data using partial least squares regression," *Wood Science and Technology* **35,** 475–485 (2001).

[15] S. S. Kelley, T. G. Rials, R. Snell, L. H. Groom, and A. Sluiter, "Use of near infrared spectroscopy to measure the chemical and mechanical properties of solid wood," *Wood Science and Technology* **38,** 257–276 (2004).

[16] T. Fujimoto, Y. Kurata, K. Matsumoto, and S. Tsuchikawa, "Feasibility of near-infrared spectroscopy for on-line grading of sawn lumber," *Applied Spectroscopy* **64,** 92–99 (2010).

[17] T.-F. Yeh, H.-M. Chang, and J. F. Kadla, "Rapid prediction of solid wood lignin content using transmittance near-infrared spectroscopy," *Journal of Agricultural and Food Chemistry* **52,** 1435–1439 (2004).

[18] F. S. Poke, J. K. Wright, and C. A. Raymond, "Predicting extractives and lignin contents in Eucalyptus globulus using near infrared reflectance analysis," *Journal of Wood Chemistry and Technology* **24,** 55–67 (2004).

[19] A. Terdwongworakul, V. Punsuwan, W. Thanapase, and S. Tsuchikawa, "Rapid assessment of wood chemical properties and pulp yield of Eucalyptus camaldulensis in Thailand tree plantations by near infrared spectroscopy for improving wood selection for high quality pulp," *Journal of Wood Science* **51,** 167–171 (2005).

[20] P. D. Jones, L. R. Schimleck, G. F. Peter, R. F. Daniels, and A. Clark III, "Nondestructive estimation of wood chemical composition of sections of radial wood strips by diffuse reflectance near infrared spectroscopy," *Wood Science and Technology* **40,** 709–720 (2006).

[21] L. Donaldson, K. Radotić, A. Kalauzi, D. Djikanović, and M. Jeremić, "Quantification of compression wood severity in tracheids of Pinus radiata D. Don using confocal fluorescence imaging and spectral deconvolution," *Journal of Structural Biology* **169,** 106–115 (2010).

[22] V. Piuri and F. Scotti, "Design of an automatic wood types classification system by using fluorescence spectra," *Systems, Man, and Cybernetics, Part C: Applications and Reviews, IEEE Transactions on* **40,** 358–366 (2010).

[23] S.-Y. Yang, Y. Han, Y.-S. Chang, K.-M. Kim, I.-G. Choi, and H. Yeo, "Moisture Content Prediction Below and Above Fiber Saturation Point by Partial Least Squares Regression Analysis on Near Infrared Absorption Spectra of Korean Pine," *Wood and Fiber Science* **45,** 415–422 (2013).

[24] L. Thygesen and S. Lundqvist, "NIR measurement of moisture content in wood under unstable temperature conditions. Part 1. Thermal effects in near infrared spectra of wood," *Journal of Near Infrared Spectroscopy* **8,** 183–189 (2000).

[25] M. L. Selbo, *Adhesive bonding of wood* (US Department of Agriculture, Washington DC, USA, 1975).

[26] R. A. Mbachu and T. G. Congleton, "Spectroscopic monitoring of resin-application prior to assembly of composite wood veneer product," (2005), US Patent 6,942,826.

[27] J. Larsson, K. Thavelin, S. Rönnbäck, T. Lagerbäck, and T. Sandin, "Apparatus, method and system for detecting the width and position of adhesives applied to a substrate," (2005), WO Patent 2,005,087,460.

[28] W. F. Huck, "Electro–optical devide for measuring thicknesses," (1956), US Patent 2,773,412.

[29] N. K. Edwards and M. W. Gorden, "Glue detection system," (1987), US Patent 4,704,603.

[30] J. T. May and E. A. Casacia, "Measurement of the thickness of thin films," (1989), US Patent 4,841,156.

[31] O. Hagman, "Multivariate prediction of wood surface features using an imaging spectrograph," *Holz als Roh-und Werkstoff* **55,** 377–382 (1997).

[32] J. Nyström and O. Hagman, "Real-time spectral classification of compression wood inPicea abies," *Journal of Wood Science* **45,** 30–37 (1999).

[33] C. M. Pieters, J. Boardman, B. Buratti, A. Chatterjee, R. Clark, T. Glavich, R. Green, J. Head, P. Isaacson, E. Malaret, T. McCord, J. Mustard, N. Petro, C. Runyon, M. Staid, J. Sunshine, L. Taylor, S. Tompkins, P. Varanasi, and M. White, "The Moon mineralogy mapper (M3) on Chandrayaan-1," *Current Science* **96,** 500–505 (2009).

[34] R. L. Easton Jr, K. T. Knox, and W. A. Christens-Barry, "Multispectral imaging of the Archimedes palimpsest," in *Applied Imagery Pattern Recognition Workshop, 2003. Proceedings. 32nd* (IEEE, 2003), pp. 111–116.

[35] M. Kim, Y. Chen, and P. Mehl, "Hyperspectral reflectance and fluorescence imaging system for food quality and safety," *Transactions of the American Society of Agricultural Engineers* **44,** 721–730 (2001).

[36] K. Heia, A. H. Sivertsen, S. K. Stormo, E. Elvevoll, J. P. Wold, and H. Nilsen, "Detection of nematodes in cod (Gadus morhua) fillets by imaging spectroscopy," *Journal of Food Science* **72,** E011–E015 (2007).

[37] G. Vane, R. O. Green, T. G. Chrien, H. T. Enmark, E. G. Hansen, and W. M. Porter, "The airborne visible/infrared imaging spectrometer (AVIRIS)," *Remote Sensing of Environment* **44,** 127–143 (1993).

[38] J. Antikainen, M. Hauta-Kasari, J. Parkkinen, and T. Jaaskelainen, "Using two line scanning based spectral cameras simultaneously in one measurement process to create wider spectral area from the measured target," in *IEEE International Workshop on Imaging Systems and Techniques - IST 2007.* (IEEE, 2007), pp. 1–5.

[39] M. E. Klein, B. J. Aalderink, R. Padoan, G. De Bruin, and T. A. Steemers, "Quantitative hyperspectral reflectance imaging," *Sensors* **8,** 5576–5618 (2008).

[40] Spectral Imaging Ltd., "Datasheet: AisaFENIX hyperspectral sensor," (2012).

[41] International Standard, "ISO 21348: Space environment (natural and artificial) – Process for determining solar irradiances," (2007).

[42] H.-C. Lee, *Introduction to Color Imaging Science* (Cambridge University Press, Cambridge, UK, 2005).

[43] M. Bass, *Handbook of optics. Vol. 2, Devices, measurements, and properties* (McGraw-Hill, New York, USA, 1995).

[44] J. W. Robinson, E. M. S. Frame, and G. M. Frame II, *Undergraduate instrumental analysis* (Marcel Dekker, New York, USA, 2005).

[45] N. Hagen and M. W. Kudenov, "Review of snapshot spectral imaging technologies," *Optical Engineering* **52,** 90901–90901 (2013).

[46] T. S. Hyvarinen, E. Herrala, and A. Dall'Ava, "Direct sight imaging spectrograph: a unique add-on component brings spectral imaging to industrial applications," in *Photonics West'98 Electronic Imaging* (International Society for Optics and Photonics, 1998), pp. 165–175.

[47] G. Blasse and B. Grabmaier, *Luminescent materials*, Vol. 44, (Springer, Berlin, Germany, 1994).

[48] J. Mutanen, *Fluorescent Colors*, PhD thesis (University of Joensuu, Joensuu, Finland, 2004).

[49] M. Ruiz-Urbieta, E. M. Sparrow, and E. R. G. Eckert, "Methods for Determining Film Thickness and Optical Constants of Films and Substrates," *Journal of Optical Society of America* **61,** 351 (1971).

[50] R. M. A. Azzam, A.-R. M. Zaghloul, and N. M. Bashara, "Polarizer–surface–analyzer null ellipsometry for

film–substrate systems," *Journal of Optical Society of America* **65,** 1464 (1975).

[51] K. Matsuda and T. Eiju, "Interferometric determination of film thickness and absolute fringe order: a new method," *Applied Optics* **25,** 2641 (1986).

[52] K. F. McCarty, "Raman scattering as a technique of measuring film thickness: interference effects in thin growing films," *Applied Optics* **26,** 4482 (1987).

[53] E. J. Hutchinson, D. Shu, F. LaPlant, and D. Ben-Amotz, "Measurement of Fluid Film Thickness on Curved Surfaces by Raman Spectroscopy," *Applied Spectroscopy* **49,** 1275 (1995).

[54] M. A. Gaon, "Detection and measurement of cold emulsion adhesives applied to a substrate," (2001), US Patent 6,281,500.

[55] J. I. Amalvya, C. A. Lasquibara, R. Arizagab, H. Rabalb, and M. Trivib, "Application of dynamic speckle interferometry to the drying of coatings.," *Progress in Organic Coatings* **42,** 89–99 (2001).

[56] B. F. Taylor, "System and method for the on-line measurement of glue application rate on a corrugator," (2002), US Patent 6,470,294 B1.

[57] R. A. Mbachu and T. G. Congleton, "Methods for monitoring resin-loading of wood materials and engineered wood products," (2005), US Patent 6,846,447 B2.

[58] S. Otsuki, K. Tamada, and S.-I. Wakida, "Two–dimensional thickness measurements based on internal reflection ellipsometry," *Applied Optics* **44,** 1410 (2005).

[59] D. Pristinski, V. Kozlovslaya, and S. A. Sukhishvili, "Determination of film thickness and refractive index in one measurement of phase–modulated ellipsometry," *Journal of Optical Society of America* **23,** 2639 (2006).

[60] J. J. Cowan and A. G. Landers, "Method using NIR spectroscopy to monitor components of engineered wood products," (2007), US Patent 7,279,684.

[61] G. Scarel, J.-S. Na, B. Gong, and G. N. Parsons, "Phonon Response in the Infrared Region to Thickness of Oxide Films Formed by Atomic Layer Deposition," *Applied Spectroscopy* **64,** 120–126 (2010).

[62] V. Lauria, J. Gillen, and R. McKinley, "Adhesive detection methods," (2012), US Patent 8,313,799.

[63] Fraunhofer-Gesellschaft, "Research news 3: Effective thermal insulation with wood foam," (2014).

[64] F. Carvalheiro, L. C. Duarte, and F. M. Gírio, "Hemicellulose biorefineries: a review on biomass pretreatments," *Journal of Scientific & Industrial Research* **67,** 849–864 (2008).

[65] S. Liu, T. E. Amidon, R. C. Francis, B. V. Ramarao, Y.-Z. Lai, and G. M. Scott, "From forest biomass to chemicals and energy; Biorefinery initiative in New York State," *Industrial Biotechnology* **2,** 113–120 (2006).

[66] M. Schwanninger, J. C. Rodrigues, and K. Fackler, "A review of band assignments in near infrared spectra of wood and wood components," *Journal of Near Infrared Spectroscopy* **19,** 287 (2011).

[67] C. D. Elvidge, "Visible and near infrared reflectance characteristics of dry plant materials," *Remote Sensing* **11,** 1775–1795 (1990).

[68] J. Soukupova, B. Rock, and J. Albrechtova, "Spectral characteristics of lignin and soluble phenolics in the near infrared – a comparative study," *International Journal of Remote Sensing* **23,** 3039–3055 (2002).

[69] J. Nyström, L. Axrup, and E. Dahlquist, "Long-term evaluation of on-line sensors for determination of moisture in biomass," (2002), Värmeforsk, Sweden.

[70] L. Axrup, K. Markides, and T. Nilsson, "Using miniature diode array NIR spectrometers for analysing wood chips and bark samples in motion," *Journal of Chemometrics* **14,** 561–572 (2000).

[71] C.-L. So, B. K. Via, L. H. Groom, L. R. Schimleck, T. F. Shupe, S. S. Kelley, and T. G. Rials, "Near infrared spectroscopy in the forest products industry," *Forest Products Journal* **54,** 6–16 (2004).

[72] A. Thumm, M. Riddell, B. Nanayakkara, J. Harrington, and R. Meder, "Near infrared hyperspectral imaging applied to mapping chemical composition in wood samples," *Journal of Near Infrared Spectroscopy* **18,** 507 (2010).

[73] T. Fujimoto, T. Numa, H. Kobori, and S. Tsuchikawa, "Visualisation of spatial distribution of moisture content and basic density using near-infrared hyperspectral imaging method in sugi (Cryptomeria japonica)," *International Wood Products Journal* (2014).

[74] S. Tsuchikawa, K. Hayashi, and S. Tsutsumi, "Nondestructive measurement of the subsurface structure of biological material having cellular structure by using near-infrared spectroscopy," *Applied Spectroscopy* **50,** 1117–1124 (1996).

[75] S. Tsuchikawa and S. Tsutsumi, "Directional characteristics model and light-path model for biological material having cellular structure," *Applied Spectroscopy* **53,** 233–240 (1999).

[76] S. Tsuchikawa and S. Tsutsumi, "Analytical characterization of reflected and transmitted light from cellular structural material for the parallel beam of NIR incident light," *Applied Spectroscopy* **53,** 1033–1039 (1999).

[77] P. Kubelka and F. Munk, "Ein Beitrag zur Optik der Farbanstriche," in *Zeitschrift für technische Physik*, Vol. 12 (1931), pp. 593–601.

[78] S. Tsuchikawa, M. Torii, and S. Tsutsumi, "Directional characteristics of near infrared light reflected from wood," *Holzforschung* **55,** 534–540 (2001).

[79] S. Tsuchikawa, "Non-traditional application of time-of-flight near-infrared spectroscopy to biological material having cellular structure," *Analytical Sciences* **17,** 1463–1466 (2001).

[80] Spectral Imaging Ltd., "Datasheet: Imspector VIS & VNIR," (2013).

[81] Spectral Imaging Ltd., "Datasheet: Imspector NIR & SWIR," (2013).

[82] Spectral Imaging Ltd., "Datasheet: Imspector UV," (2009).

[83] Spectral Imaging Ltd., "Test Report: Imspector V10E," (2006).

[84] Spectral Imaging Ltd., "Test Report: Imspector N25E," (2009).

[85] Spectral Imaging Ltd., "Test Report: Imspector UV4E," (2009).

[86] L. Karlman, T. Mörling, and O. Martinsson, "Wood Density, Annual Ring Width and Latewood Content in Larch and Scots Pine," *Eurasian Journal of Forest Research* **8,** 91–96 (2005).

[87] W. T. Simpson, Chap 12 Drying and control of moisture content and dimensional changes in *The Encyclopedia of Wood* (Skyhorse Publishing Inc., New York, USA, 2013).

[88] A. Field, *Discovering statistics using SPSS (and sex and drugs and rock n roll)* (SAGE Publications Ltd, London, UK, 2009).

[89] A. Buades, B. Coll, and J.-M. Morel, "A review of image denoising algorithms, with a new one," *Multiscale Modeling & Simulation* **4,** 490–530 (2005).

[90] R. R. Shannon and J. C. Wyant, *Applied Optics and Optical Engineering* (Academic Press Inc., New York, USA, 1983).

[91] H. H. Willard, L. L. Merritt, J. A. Dean, and F. A. Settle, *Instrumental methods of analysis* (Wadsworth, Belmont, USA, 1988).

[92] R. J. Marks, *Handbook of Fourier analysis & its applications* (Oxford University Press, London, UK, 2009).

[93] G. Yang, C. V. Stewart, M. Sofka, and C.-L. Tsai, "Registration of challenging image pairs: Initialization, estimation, and decision," *Pattern Analysis and Machine Intelligence, IEEE Transactions on* **29,** 1973–1989 (2007).

[94] C. V. Stewart, C.-L. Tsai, and B. Roysam, "The dual-bootstrap iterative closest point algorithm with application to retinal image registration," *Medical Imaging, IEEE Transactions on* **22,** 1379–1394 (2003).

[95] Å. Rinnan, F. V. D. Berg, and S. B. Engelsen, "Review of the most common pre-processing techniques for near-infrared spectra," *TrAC Trends in Analytical Chemistry* **28,** 1201–1222 (2009).

[96] J. X. Wu, S. Rehder, F. van den Berg, J. M. Amigo, J. M. Carstensen, T. Rades, C. S. Leopold, and J. Rantanen, "Chemical imaging and solid state analysis at compact surfaces using UV imaging," *International Journal of Pharmaceutics* **477,** 527–535 (2014).

[97] K. H. Norris and A. M. C. Davies, "Examining diffuse reflection and transmission spectra more thoroughly: Part 1. Instrument noise," *Spectroscopy Europe* **23,** 24–27 (2011).

[98] M. F. Modest, *Radiative heat transfer* (Academic Press, Oxford, UK, 2013).

[99] R. Kane and H. Sell, *Revolution in lamps: a chronicle of 50 years of progress* (The Fairmont Press Inc., Lilburn, USA, 2001).

[100] Z. Al-Ameen, G. Sulong, and M. G. M. Johar, "A comprehensive study on fast image deblurring techniques," *International Journal of Advanced Science and Technology* **44** (2012).

Tapani Hirvonen

A Wide Spectral Range Imaging System - Applications in Wood Industry

This study introduces a new wide spectral range imaging system with photoluminescence imaging capability. The system is benchmarked and applied to two research cases in the context of the wood industry. The first research case is the acquisition of a public spectral image database of sawn timber which potential is demonstrated with an analysis examples. The second research case is the development of a non-destructive method for layer thickness measurement of freshly applied water-dilutable compounds.

UNIVERSITY OF EASTERN FINLAND

Publications of the University of Eastern Finland
Dissertations in Forestry and Natural Sciences

ISBN 978-952-61-1725-6